Biomedical overview of melanin. 2. Updating molecular modeling, synthesis mechanism, and supramolecular properties regarding melanoma therapy

Juan Carlos STOCKERT[1,2,*]; Alfonso BLÁZQUEZ-CASTRO[3]

[1] Facultad de Medicina, Instituto de Oncología "Angel H. Roffo", Universidad de Buenos Aires, Buenos Aires, C1417DTB, Argentina
[2] Centro Integrativo de Biología y Química Aplicada (CIBQA), Universidad Bernardo O'Higgins, Santiago, 8370854, Chile
[3] Departamento de Biología, Facultad de Ciencias, Universidad Autónoma de Madrid, Madrid, 28049, Spain

Abstract: Melanins represent one of the most ancient and important group of natural macromolecular pigments. They have multiple biological roles in almost all organisms across the Phyla, examples being photoprotection, anti-oxidative action, radical scavenger activity, and heavy metal removal. From the biomedical point of view, melanocytes are involved in the origin of melanoma tumors, and the main therapeutic advances for their treatment have been revised in Part 1 of this review. The chemical structure of eumelanin is a biological concern of great importance, and therefore, exploring theoretical molecular models and synthesis mechanisms will be here described, as well as molecular orbital features and supramolecular organization, which are responsible for the key properties that make these biological pigments so important, and so fascinating. Ultimately, this updated overview is devoted to describe present structural models and physico-chemical characteristics of eumelanin, in order to explain and utilize melanin properties on which new photothermal and ultrasonic protocols for melanoma treatment can be devised and applied.

Introduction

Melanin is a rather descriptive term that denotes a black pigment of biological origin, but at present, it is accepted that it corresponds to a definite group of indole and catechol biopolymers. Melanin is considered one of the most ancient pigments widely found in the two domains of life, namely Prokaryota and Eukaryota, the last including the kingdoms Protista, Fungi, Plantae, and Animalia (Nicolaus *et al.*, 1994; Land *et al.*, 2004; d'Ischia *et al.*, 2015; D'Alba and Shawkey, 2019; Martínez *et al.*, 2019). The precise chemical structure of animal melanins is still poorly known, although overwhelming evidence indicate that they are formed by an indole polymer with high conjugation degree, which is related to their strong photon absorption and other physico-chemical features.

Following the first part of this review (Blázquez-Castro and Stockert, 2021), in this second part emphasis will lay on several proposed structural models, chemical synthesis, supramolecular organization and properties of eumelanin. Indole-type eumelanin is brown-black (in mammals, cuttlefish, etc.), and pheomelanin is yellow-red (in red hair and feathers). In plants and fungi, melanins commonly correspond to the catechol-type, and generally they are named allomelanins (Land *et al.*, 2004; Zhou *et al.*, 2019). In human melanosomes, melanin appears as formed by a pheomelanin core produced first, followed by a eumelanin shell deposited on the surface (the casing model), their ratio determining skin and hair color (Simon *et al.*, 2008). Taking into account that pheomelanin is of relevant concern in melanin biology and pathology, a more specific contribution about pheomelanin will be published as Part 3 of this overview series on melanin and melanoma.

Although melanin is generally produced in melanosomes, neuromelanin (NM) from nervous structures like *substantia nigra*, *locus coeruleus*, *stria vascularis*, etc. (Nicolaus, 2005b) differs in that its biosynthesis does not take place within this organelle (Simon *et al.*, 2008). NM is a Fe^{3+}-rich insoluble pigment originated from dopamine-derived quinones contained in autophagic lysosomes, together with lipids. The melanin component is bound to cross-β-sheet peptides and

*Address correspondence to: Juan Carlos Stockert,
jcstockert@fvet.uba.ar

aliphatic dolichols chains, which are the main components of lipid bodies within the NM-containing cell structure (Sulzer et al., 2018). In mammals, the retinal pigment epithelium has also a complex organization, with melanosomes, lipofuscin, and melanosomes encased in lipofuscin that are called melano-lipofuscin granules (Simon et al., 2008).

Melanins are very relevant compounds in biomedicine. They are antioxidants and detoxification agents, acting by removing reactive oxygen species (ROS), radicals, toxic heavy metals, and harmful chemicals. The conjugated structure of natural and synthetic melanins allows easy redox changes and equilibrium between quinone and catechol groups (Sarangarajan and Apte, 2006). These groups are also involved in binding to metal cations (Nicolaus, 1997; d'Ischia et al., 2015), and provide strong adhesiveness to other molecules and surfaces (Ruiz-Molina et al., 2018; Chen et al., 2021).

Melanin also characterizes the malignant melanoma, which is one of the most aggressive human tumors. Although a significant progress has been achieved for melanoma treatments involving cytokines, check point and kinase inhibitors, immuno-, genic-, and combinational-therapies (Berrios-Colon and Williams, 2012; Rughani et al., 2013; Achkar and Tarhini, 2017; Finocchiaro et al., 2019; Wang et al., 2020), successful protocols are still difficult in the case of the advanced disease (Ahn et al., 2017; Domingues et al., 2018; Naidoo et al., 2018; Li et al., 2020), and further studies on new therapeutic modalities based on chemical and physical approaches are still necessary.

New melanoma treatments need to be based on a deeper understanding of the molecular structure of melanin. Therefore, the aim of the second part of this review, in agreement with suggested rules and criteria for review articles (Cranford, 2021), is to update and propose chemical structures and synthesis mechanisms of eumelanin, as well as its supramolecular organization and properties, attempting to offer seminal perspectives for innovative therapeutic conceptions and further developments.

Chemical Structure

Previous and recent reviews on different chemical models of eumelanin have been published (Prota, 1997; Bridelli, 1998; Meng and Kaxiras, 2008; Liebscher et al., 2013; Micillo et al., 2016; Panzella et al., 2018; Blázquez-Castro and Stockert, 2021; Stockert, 2021), but at present no agreement has been reached yet regarding its precise chemical structure. High molecular weight, low or null solubility in water and organic solvents, resistance to hydrolysis, and some heterogeneity between samples difficult the structural analysis. In spite of these limitations, several polymeric linear models have been proposed (Fig. 1). Simpler models have been already described in the first part of this review (Blázquez-Castro and Stockert, 2021).

Common research on eumelanin chemical structure has been performed by analysis of fragmented products, and less attention has been devoted to the application of physical methods. However, studies based on X-ray crystallography and electron microscopy have shown that amorphous samples of synthetic and natural eumelanins have a multilayer (graphite-like) structure (Thathachari and Blois, 1969; Bridelli et al., 1990; Watt et al., 2009; Chen et al., 2013), which explains most physico-chemical properties of this supramolecular solid-state material (Nicolaus, 1997; Olivieri and Nicolaus, 1999).

Melanin precursors are the following: (a) for eumelanin, tyrosine and/or 3,4-dihydroxy-phenylalanine (DOPA); (b) pheomelanin is produced from tyrosine and/or DOPA in the presence of cysteine; (c) allomelanins form using 4-hydroxy-phenylacetic acid, catechols, 1,8-dihydroxy-naphthalene (DHN), caffeic acid, etc., and (d) pyomelanin of micro-organisms results from homogentisic acid (Lindgren et al., 2015;
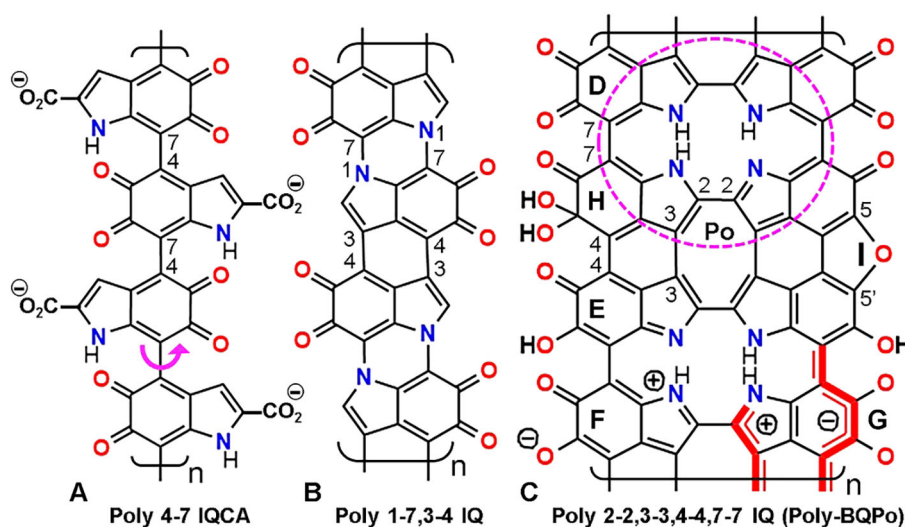

FIGURE 1. Formal structure of linear eumelanin polymers with atom numbering. Note that rotation freedom of indole rings only occurs in poly 4-7 IQCA (A) (curved arrow). In contrast, poly 1-7,3-4 IQ (B) and poly-BQPo (C) have more than one bond between successive indoles, and then they are more rigid and planar. The porphycene ring Po is shown as a dashed ellipse. Non-ionic mesomer (D), imino-semiquinone (E), ionic (F), and π* conjugated ionic form (G) are indicated, as well as the hydrated IQ unit (H), and the 5,5'-ether bridge from two indole units (I). Structures are shown according to the models: poly 4-7 IQ (Liebscher et al., 2013; d'Ischia et al., 2015); poly 1-7,3-4 IQ (Meredith and Sarna, 2006); poly-BQPo (Olivieri and Nicolaus, 1999; Stockert, 2021).

Martínez et al., 2019; Lorquin et al., 2021). Most fungal melanins are polymers of DHN, but some fungi can also utilize tyrosine, catechol, catecholamines, etc., and thus correspond to eumelanins (Eisenman and Casadevall, 2012; Cordero and Casadevall, 2017; Camacho et al., 2019). Opiomelanins are another group of indole pigments related to opioid peptides (enkephalins) (Mosca et al., 1999).

In vertebrates, eumelanin is formed from L-tyrosine through enzymatic and spontaneous chemical reactions known as the Raper–Mason pathway (Prota, 2000; Simon et al., 2008; Borovanský and Wiley, 2011), and involves oxidation of tyrosine by tyrosinase to DOPA, followed by DOPA quinone, and then to 5,6-dihydroxyindole-2-carboxylic acid (DHICA) and 5,6-dihydroxyindole (DHI) (Edelstein, 1971; d'Ischia et al., 2015), which is the most versatile precursor.

DHICA and DHI can be oxidized and/or decarboxylated forming indole-5,6-quinone (IQ). From these precursors (shown here as DHI or IQ units), different dimers (e.g., bis 3-4 IQ, bis 4-7 IQ, bis 7-7 IQ, and bis 2-2 IQ [trans and cis, according the N site]) can be formed. The cyclic tetramer 2-7 IQ is a benzoquinone porphyrin (BQP). The structure of several possible IQ dimers and cyclic tetramers has been reviewed (Blázquez-Castro and Stockert, 2021; Stockert, 2021).

Flexible and rigid linear polymers are illustrated in Fig. 1. Note that bis-BQPo (tetra 2-2,3-3,4-4,7-7 IQ) corresponds to a benzoquinone derivative (BQ) of the porphycene ring (Po), which is a structural isomer of the porphyrin ring (Arad et al., 2002; Stockert et al., 2007). The eumelanin unit IQ (Fig. 1(C)) can adopt several mesomeric forms, in equilibrium between the formal uncharged unit (Fig. 1(D)), and the non-ionic (E), ionic (F) and excited mesomer (G). The latter corresponds to the $\pi^\star$ conjugated ionic form, which represents the first excited singlet state (S_1). This is the case of several dyes, in which the ionic- and non-ionic dye mesomers correspond to the excited (high energy) and ground (low energy) states, respectively (Nagasawa et al., 2001). IQ units can also suffer a reversible hydration at the 5-keto group (Bishop and Tong, 1964) (Fig. 1(H)), and metal ions chelation by oxygen ligands. Dehydration of DHI generates a 5,5'-ether bridge and a furan group between indole units (Fig. 1(I)) (Olivieri and Nicolaus, 1999).

Synthesis Mechanism

According to the fossil record, melanins are very ancient biopigments (biochromes) (Lindgren et al., 2015). It is tempting to speculate that on account of the easy spontaneous and non-enzymatic polymerization of catechols and indolequinones, melanins could have been one of the first aromatic macromolecules on the earth. In addition to enzymatic synthesis, melanin-like compounds are spontaneously formed in vitro at slight alkaline pH by oxidative polymerization of several precursors such as DOPA, dopamine (DA), DHI, IQ, adrenalin, serotonin, 5,6-dihydroxy-tryptamine, etc. (Dreyer et al., 2012; Micillo et al., 2016). Synthetic melanins do not contain protein components, and thus they are more suitable for biomedical and biotechnological applications. X-rays studies indicate that synthetic polydopamine-(PDA)-melanin, and

tyrosine-melanin are essentially similar to natural eumelanin in their local atomic arrangements (Cheng et al., 1994).

Interestingly, self-assembly of aromatic building blocks to form organic polymers is a well-known process (Li et al., 2013). Self-assembly is promoted by face-to-face π–π stacking (Ryu et al., 2008; Ma et al., 2020), and it could occur in the spontaneous polymerization of melanin. A progressive self-assembly of precursors based on cation–π interactions has been suggested (Hong et al., 2018), using ammonium, Na+ and K+ ions to illustrate the assembly mechanism. Although the described process agrees with the broad absorption spectra of natural or synthetic eumelanins, it does not account for their well-known graphitic (multilayer) structural organization.

Under oxidative conditions, H atoms can be easily removed from phenolic -OH groups, which is a widely known chemical process (Krieg et al., 2007). In the case of indole and catechol precursors, polymerization can take place through O and C radicals (Zhou et al., 2019). After H removal, atoms with unpaired electrons (O• and C•) are intermediates in the oxidative polymerization of DHI units (Fig. 2). H atoms can be abstracted directly from =CH- and -NH- groups by previously generated O radicals (hydroxyl, superoxide, peroxyl). Highly reactive N• and C• radicals at positions 1, 2, 3, 4, and 7 can bind in out-of-plane reactions, forming C-C and C-N covalent bonds between indole precursors (Figs. 2(A)–2(D)). It is known that C atoms at 2,3,4, and 7 sites are the most reactive in the indole ring (Nicolaus, 1997).

Easy auto-assembly processes can be based on stacking of DHI or IQ monomers forming a scaffold for polymerization. Following molecular modeling studies on the stacking of dyes
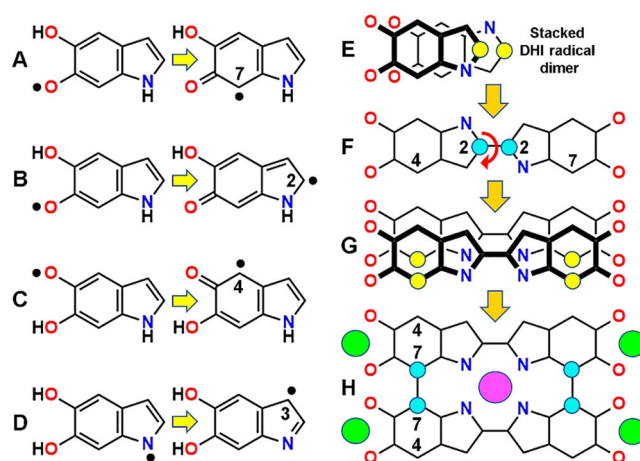

FIGURE 2. Possible synthesis mechanism of poly-BQPo. (A, B, C, D) Radicals formed in DHI from removal of H atoms bound to O or N atoms (left), and then transferred to C atoms (C•, right), allowing C–C bonding. (E, F, G, H) Stacked DHI O-cis/N-trans radical dimer (E) to form bis-DHI (F), stacked bis-DHI radical dimer (G), and BQPo (H). Energy minimization of the face-to-face stacked DHI dimer (E) was made with HyperChem 7, MM+ converged to 0.1 kcal/(Å mol). Formation of dimers (large arrows) occurs by rolling of thick-over-thin precursors and dimer units. Radical and bound C atoms are shown as yellow and cyan circles, respectively. Curved arrows indicate where rotation freedom of C–C bonds exists. Relevant atom numbers are indicated. Binding of metal cations to O (green) and N (violet) sites are indicated.

(Stockert and Abasolo, 2011), the comparison between stacked dimers of IQ or DHI precursors shows that the O-*cis*-N-*trans* DHI dimer (Fig. 2(E)) have the lowest free energy (kcal/mol) for triggering dimerization. Other configurations of dimers with suitable low energy are also possible (e.g., O-*trans*/N-*trans* DHI). This radical-based process results in the formation of a double-stranded IQ chain (poly-BQPo) (Figs. 2(F)–2(H)), but also the poly 4-7 IQ chain can be formed by this mechanism.

Obviously, this is a simplistic representation of a more complex molecular process, but the results of these exploring synthesis mechanisms allow to illustrate the kind of process that could lead to spontaneous melanin synthesis. Taking into account the abundant precedents in the self-assembly of polymers based on radical formation and face-to-face stacking, a reasonable spontaneous polymerization to form eumelanin would involve stacked IQ or DHI precursor radicals as shown in Fig. 2.

However, eumelanin biosynthesis and melanosome biogenesis represent more complex and regulated processes than spontaneous synthesis. Enzymes, structural scaffolding proteins, metal ions, and acidic pH are key factors in eumelanin formation in living melanocytes (D'Alba and Shawkey, 2019; Wiriyasermkul *et al.*, 2020), also involving interactions of the growing polyanionic melanin polymer with positively charged surfaces of basic melanosome proteins (Sarangarajan and Apte, 2006). Signaling pathways and regulation of enzymatic melanogenesis in mammals have been reviewed (Wasmeier *et al.*, 2008; D'Mello *et al.*, 2016).

Molecular Modeling

Exploring theoretical structures by molecular modeling has become an important task to attempt advances in understanding the organization of natural and synthetic melanins (Galvão and Caldas, 1990; Tran *et al.*, 2006; Meng and Kaxiras, 2008; Chen *et al.*, 2013; Chen *et al.*, 2014). Regarding the basic structure of eumelanin, three types of molecular models can be taken into account, namely monomer and cyclic oligomers, flexible chains, and rigid chains. There are assets and opposing views for each of these structural models. In most cases, they will be presented in the oxidized IQ forms.

Monomer and cyclic oligomer models

Simple H-bond aggregates of isolated indole monomers (Dreyer *et al.*, 2012) have a very low conjugation degree, and thus the broad-band absorption spectra of eumelanin cannot be easily explained. Massive chromophore stacking and π-interactions occur in aromatic compounds either in solution or solid state (e.g., tri- and macrocyclic dyes, as well as stacked base-pairs in nucleic acids), but they have no broad-band absorption but well-structured spectra (Stockert and Blázquez-Castro, 2017). Therefore, models of eumelanin only based on stacking of isolated indole units seem unlikely (Stockert, 2021).

IQ cyclization gives the 2-7 IQ tetramer or benzoquinone-porphyrin (BQP) (Kaxiras *et al.*, 2006; Meng and Kaxiras, 2008). However, it is again not expected that only stacking of these structures without extensive covalent conjugation could explain spectral properties. Indeed, if the molecular structure of eumelanin is non-covalent and only

based on hydrophobic and/or H-bonding forces, then solubilization and bleaching of the pigment should occur by treatment with organic solvents and H-bond disrupting agents (e.g., urea, formamide), and this is not the case.

It must be noted that instead of planar stacking of cyclic IQ tetramers, helical stacking of a linear continuous polymer has been suggested as an alternative melanin model (Meng and Kaxiras, 2008). The helix is formed by connecting successive tetramers through 2-7 bonds, with the fifth monomer stacked directly above the first, but without an adequate scaffold, the formation of this helical model is rather difficult to explain. Other planar cyclic or irregular oligomers containing 5-8 indole units have been also proposed as eumelanin models (Zajac *et al.*, 1994; Arzillo *et al.*, 2010; Chen *et al.*, 2014). A tetra-indole model formed by two DHI and two IQ monomers linked by two amide groups between N1 and C2' has been suggested for eumelanin (Schroeder *et al.*, 2015).

On the other hand, a mixed model combining stacked monomers (Dreyer *et al.*, 2012) and covalent chains (d'Ischia *et al.*, 2015) has become fashionable. In this model, a stacked DA-DHI-DA physical trimer together with two linear zig-zag 2-2, 4-7 DHI trimers was shown as the molecular structure of PDA-melanin (Hong *et al.*, 2012; Hong *et al.*, 2018, Hauser *et al.*, 2020). Again, it seems difficult that this model could explain the main properties of the synthetic polymer, as mentioned above.

Flexible chain models

A melanin-like, zig-zag chain of 2-2,3-3 indoles, named "indole black", was suggested by Berlin (quoted by Nicolaus (1997)), but on account of steric hindrance, torsional angles of indole rings have 58° and the polymer is not planar. However, it is worth to note that free rotation of the 2-2 and 3-3 bonds can just form the BQPo ring. Likewise, a flexible 3-7 IQ chain has been proposed for eumelanin (Raghavan *et al.*, 1990), with dihedral angle of ~20°.

In the case of 2-4,2-7 DHI or IQ polymers, the chain takes up a zig-zag way with a dihedral angle of ~18° between indole rings, allowing considerable π-stacking and almost a planar configuration (Micillo *et al.*, 2016; Panzella *et al.*, 2018). Linear poly 4-7 IQ and poly 4-7 IQCA chains are the most frequently shown flexible models (Liebscher *et al.*, 2013; d'Ischia *et al.*, 2015; Micillo *et al.*, 2016; Panzella *et al.*, 2018), with an angle of ~40° between IQ units, which becomes smaller (~20°) in the first excited state, allowing greater conjugation (Blázquez-Castro and Stockert, 2021).

Regarding the still poorly known 3D organization of these eumelanin models, there are different views according to the polymer. Stacking of flexible linear or zig-zag chains (d'Ischia *et al.*, 2015; Liebscher *et al.*, 2013), or bundling arrays of flexible linear chains have been proposed (Micillo *et al.*, 2016; Panzella *et al.*, 2018), but these models do not agree with the graphitic structure detected by both X-ray crystallography and electron microscopy.

Rigid chain models

Fused indole rings have been described to form a possible rigid polymer. A curved planar eumelanin model based in the formation of 2-7 and 3-4 bonds, followed by decarboxylation at

5 and 6 positions has been proposed by Swift (2009). An intriguing feature of this fused model is the absence of catechol or quinone groups, which do not allow the typical redox possibilities of eumelanin. A rigid oligomer based on a 1-7,3-4 IQ (see Fig. 1(B)) with a planar structure has been also suggested as a eumelanin model (Meredith and Sarna, 2006). In this case, a polymeric structure with suitable stacking and extended π conjugation is possible.

A very attractive double IQ chain for eumelanin was early suggested by Olivieri and Nicolaus (1999). This structure can be formulated as poly 2-2,3-3,4-4,7-7 IQ, and then the unit of this polymer is a tetra-benzoquinone (BQ) derivative of porphycene (Po) (see Fig. 1(C), and Fig. 3(A)). Therefore, this model can be simply named poly-BQPo. The Po ring and derivatives, as well as several metal complexes (e.g., Ni, Cu, Zn, Pd) are planar unsaturated macrocycles (Arad et al., 2002; Stockert et al., 2007).

The possibility that a planar BQPo unit could be the precursor of both natural and synthetic eumelanins is amazing (Stockert, 2021). Some authors have already indicated that a component of eumelanin could be BQPo (Bridelli et al., 1990) and similar indole derivatives (Zajac et al., 1994; Arzillo et al., 2010). In contrast with linear or zig-zag flexible chains, the BQPo model fulfills the main characteristics of eumelanin as a supramolecular solid (stacked multilayered graphite-like material), explaining its broad-band absorption, photoconductivity, photothermal decay with efficient heat production, and crystallographic and electron microscopical features. Therefore, it is tempting to assume that among the speculative models suggested for eumelanin, poly-BQPo could be the most plausible (Stockert, 2021), showing similar structure and properties to those of graphene oxide and graphite oxide (Dreyer et al., 2010).

Molecular Orbitals

Inspection of molecular orbitals (MOs) allows a better understanding of the conjugation changes induced by photo-excitation (Stockert and Blázquez-Castro, 2017). MOs examples of flexible and rigid models have been described (Blázquez-Castro and Stockert, 2021; Stockert, 2021). The highest-occupied (HOMO), and lowest-unoccupied (LUMO) molecular orbitals represent the energy levels of the ground and excited molecule, respectively. In HOMO-d and LUMO+d, d is from 0 to the maximum energy level, and the HOMO-LUMO separation corresponds to the prohibited Fermi's band gap energy (Eg) between the valence band (VB) and conduction band (CB) of semiconductors. The orbital phases are denoted by colors or signs of orbital lobes. Fused lobes with the same color are in-phase, and those with isolated lobes and different color are out-of-phase. In MO images, positive and negative signs have nothing to do with charge.

Regarding the BQPo model (Fig. 3(A)) (Stockert, 2021), it must be noted that ground and excited molecules with bonding (π) and anti-bonding (π*) electron states (S$_0$ and S$_1$, respectively), result in different MOs. The excited LUMO+0 of tetra-BQPo (Fig. 3(D)) has a more extended π-conjugation (longitudinal lobes) than that of the ground HOMO-0 (rather transversal lobes) (Fig. 3(B)). In this model, the energy levels of excited states result in a compact overlapping of the LUMO "block", similar to the CB of semiconductors (Fig. 3(C)).

The same is valid for tetra 4-7 IQ, which has a clear longitudinal direction of LUMO+0 (Stockert, 2021). The increase of absorption and dark color of the DHI-melanin by further oxidation is explained by conversion of catechols to quinones (Micillo et al., 2016; Panzella et al., 2018), generating a long LUMO pattern. It is assumed that in pigments with high number of linear *ortho*-benzoquinones, black color and broad-band absorption spectra are closely related to the high π*-conjugation and longitudinal LUMO components, with low Eg and high semi-conductivity. However, in the curved fused poly 2-7,3-4 IQ (Swift, 2009), and zig-zag poly 2-4 IQ models there is no continuous LUMO, at least at low energy levels.
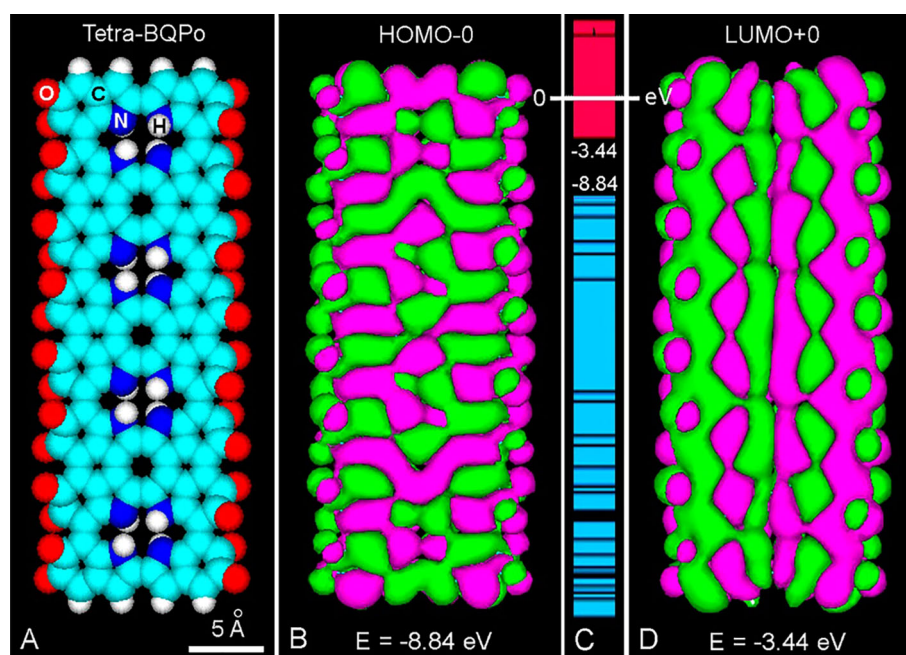

FIGURE 3. (A) Frontal view of an atomic volume model of tetra-BQPo. (B, D) Comparison between HOMO-0 (B) and LUMO+0 (D) patterns, showing positive (green) and negative (violet) π-orbital lobes with energy (E) values. (PM3 geometry optimization: 0.1 kcal/(Å mol), Gouraud shaded 3D isosurface, orbital contour: 0.00035). (C) Energy levels, showing the HOMO-0/LUMO+0 energy gap (Eg = 5.4 eV) from –8.84 eV to –3.44 eV, respectively, and the massive occurrence of LUMO excited states (CB, red) and HOMO states (VB, blue).

In other compounds such as poly 2-2 *ortho*-benzoquinones, the vicinal carbonyl-methine groups (=HC-CO-CO-CH=) also shows the extended LUMO pattern. It is noteworthy that conductivity based on polyene "spines" in organic polymers was early suggested (Little, 1964), and these spines just correspond to the extended LUMO pattern. Not only linear LUMOs are possible, circular (closed) LUMO+0 patterns also appear in *o*-quinone compounds such as *o*-quinone oligo-helicene (Gingras, 2013), hexa *o*-quinone coronene, benzo-dodeca-quinone porphycene, and cyclic penta-BQPoe.

Although the precise structure of allomelanins is still poorly known, poly 1,8-dihydroxy-naphthalene (Zhou et al., 2019; Cavallini et al., 2020) seems to be the most accepted model. A continuous LUMO+0 pattern is observed in naphthalenequinone oligomers suggested for the structure of allomelanins. It must be noted that in the allomelanin bis-benzoquinone dimer, its hydrated and ether derivatives, and the hybrid hydroxy-quinone show a continuous LUMO+0. The presence of ether groups in BQPo (BQPoe) (see Fig. 1(I)), induces curvature and facilitates extended LUMOs.

In hydrophobic face-to-face stacked aromatic compounds, π–π interactions take place resulting in either unfused or fused orbitals. Overlap of LUMOs from stacked structures depends on the energy level of the excited state. Fig. 4 illustrates a stacked BQPoe dimer, showing the different LUMO pattern at low and high energy. This feature represents the possibility of strong π–π interactions not only along the conjugated polymer but also between stacked aromatic units.

Supramolecular Organization

It must be emphasized that all the physico-chemical and biomedical properties of melanins are just the consequence of their chemical structure and supramolecular organization. The latter name involves all the features related not only to the molecule but also to the macromolecule as a solid-state material. A precise knowledge of these structural aspects (even far of complete) becomes undoubtedly necessary to understand melanin properties and applications.

In addition to the dark color and broad-band absorption spectrum, one of the most noteworthy characteristics of melanins is the multilayer appearance under transmission electron microscopy (TEM), and the molecular spacing between layers detected by X-ray crystallography. An interlayer spacing of ~3.4 Å for eumelanins and ~4 Å for allomelanins is the most commonly reported morphological parameter (Thathachari and Blois, 1969; Cheng et al., 1994; Watt et al., 2009; Chen et al., 2013). If a planar indole polymer such as poly-BQPo is the main structure of eumelanin, then a typical graphite-like organization of stacked aromatic layers would be observed by TEM. In accordance with this, ultrastructural studies show that stacked multilayers with spacing of ~3.4 Å is just the pattern observed in natural and synthetic eumelanins. It is difficult to conceive how other models (H-bound monomers, cyclic tetramers, zig-zag and linear flexible polymers) could explain the graphite-like appearance of eumelanin.

Interestingly, after formation of ether bridges by dehydration of 5 and 6 hydroxyls, the planar chain of oligo-BQPo acquires furan rings and becomes curved (Fig. 5), a feature that was early shown by Olivieri and Nicolaus (1999) using molecular modeling.

It is somewhat surprising that a small change such as the addition of ether bridges into BQPo units can modify so much the geometry of the oligomer to a curved chain. Large longitudinal and mild transversal curvatures occur in this model. When one ether group appears for every O atom, the O_{ether}/O_{total} ratio (ether index, EI) is 1/1 = 1. With 1/2 and 1/5 ratios, EI = 0.5 and 0.2, respectively. The curvature is greater with EI values between 0.5 and 1, whereas it is reduced or absent with EI between 0.2 or 0.

It is worth to note that for BQPoe oligomers, Eg values reduce when ether bridges increase. Taking into account the soft or marked curvature of oligo-BQPoe, cyclic or spiral arrangements of chains would be a logical consequence. A cyclic fullerene-like, tetra-BQPoe (16-indole) protoparticle has been early modeled for DHI-melanin (Olivieri and Nicolaus, 1999; Nicolaus, 2005a). In keeping with this, a cyclic penta-BQPoe (20-indole) represents an improved (and stable) ring structure with radial and annular HOMO-0 and LUMO+0 patterns, respectively (Fig. 6).

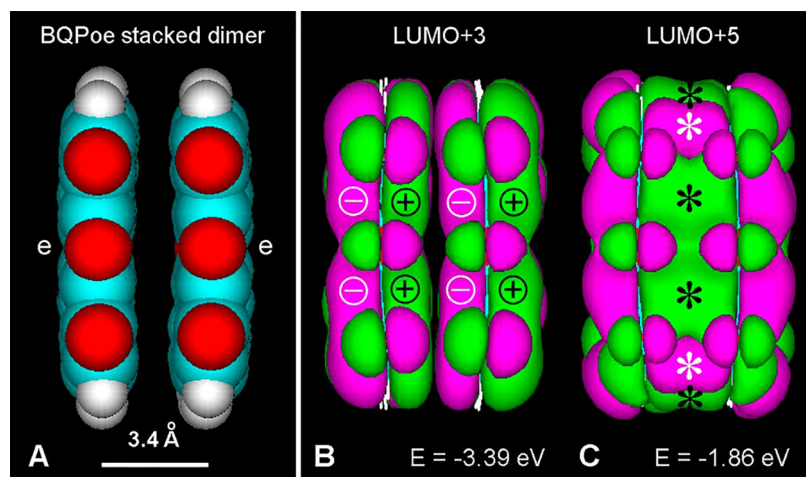It is evident that a spiral organization of stacked BQPo sheets could also form the protoparticle (Fig. 7). A BQPoe

FIGURE 4. (A) Lateral view of a BQPoe face-to-face stacked dimer (atomic volume) after PM3 geometry optimization converged at 1 kcal/(Å mol). Color code for elements as in Fig. 3. (e: ether bridges). (B, C) LUMO+3 and LUMO+5, respectively (Gouraud shaded isosurface, orbital contour value: 0.005). Observe unfused MOs of the stacked dimer at low energy (B), and fused MOs (asterisks) at higher energy (C).
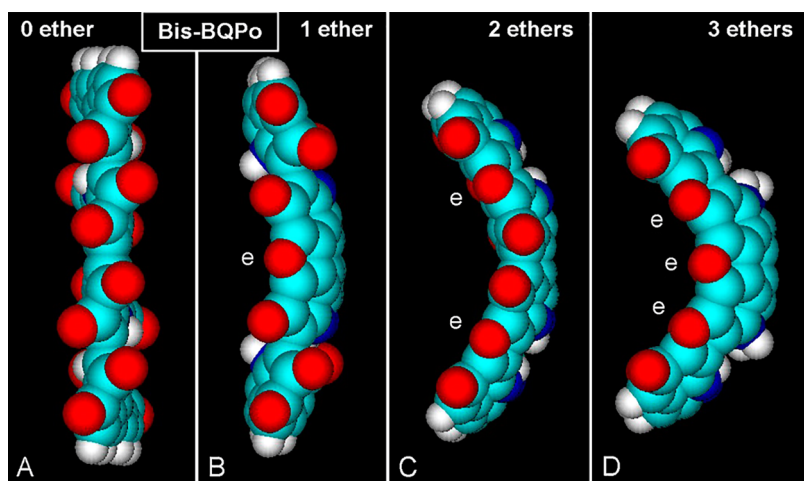
FIGURE 5. (A–D) Lateral views of atomic volume bis-BQPo models showing different curvature degrees caused by ether (e) bridges. PM3 optimization converged at E = 0.1 kcal/(Å mol). (A) Bis-BQPo without any ether bridge shows no curvature. (B, C, D) The molecules clearly show longitudinal and transversal curvatures, which are greater with increasing number of ether bridges. For element colors see Fig. 3.
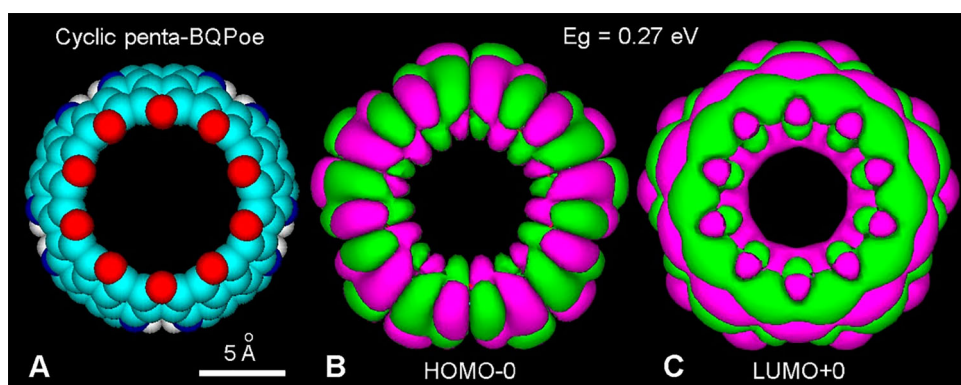

FIGURE 6. (A) Atomic volume model of a fullerene-like cyclic penta-BQPoe. All O atoms form ether bridges (EI = 1). For element colors see Fig. 3. (B, C) HOMO-0 (–10.23 eV) and LUMO+0 (–9.96 eV) showing radial and annular patterns, respectively (PM3 method, converged at 10 kcal/(Å mol), and extended Hückel, Gouraud 3D isosurface, orbital contour: 0.0003, Eg = 0.27 eV).
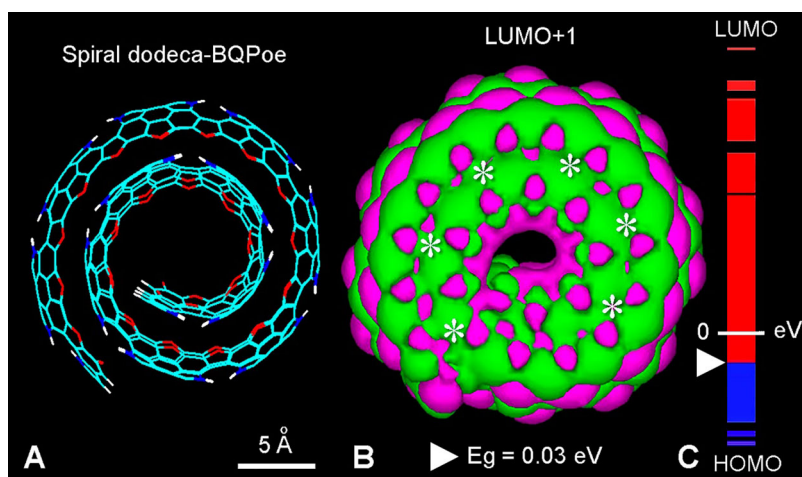

FIGURE 7. (A) Lateral view of a helical wire structure of two complete spires of a dodeca-BQPoe model with EI = 1. For element colors see Fig. 3. (B) LUMO+1 showing the annular fused pattern (asterisks) (MM + method, converged at 0.1 kcal/(Å mol), followed by extended Hückel method; Gouraud 3D isosurface, orbital contour: 0.0001; Eg (white triangle) = 0.03 eV). (C) HOMO-LUMO energy levels of dodeca-BQPoe, showing the small energy gap from HOMO-0 (–9.88 eV) to LUMO+0 (–9.85 eV), and the massive occurrence of LUMO states (CB, red) and HOMO states (VB, blue).

dodecamer forming two spiral turns is illustrated in Fig. 7(A). The LUMO+1 image (Fig. 7(B)), clearly shows a spiral pattern with fused MO lobes, and the in-block distribution of HOMO and LUMO energy levels (Fig. 7(C)).

The formation and growth of a spiral growing structure for an oligo-BQPoe is shown in Figs. 8(A) and 8(B). From a mechanistic point of view, an isolated planar chain would first begin to add ether bridges to curve it, curvatures then increase and continue, resulting in a spiral rolling model (Figs. 8(B) and 8(C)).

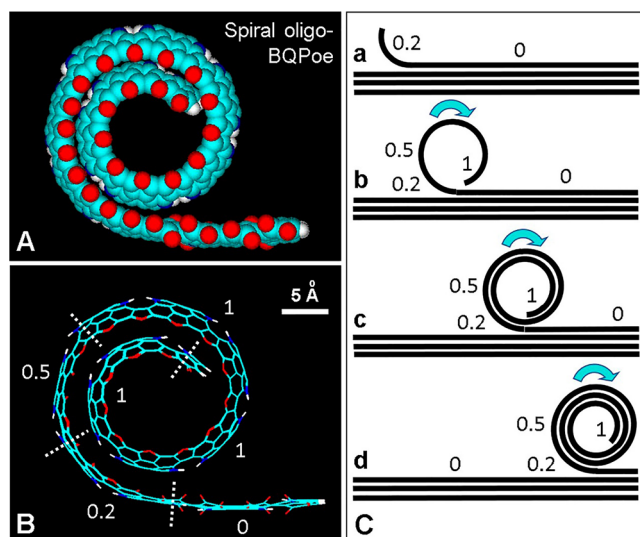Interestingly, although chemists were early predisposed to think of graphitic structures as flat sheets with sp^2 C

FIGURE 8. Spiral model of the possible organization of curved regions of eumelanin. (A) Lateral view of an atomic volume model of the spiral oligo-BQPoe with about 1.5 spires. For element colors see Fig. 3. (B) Wire structure of (A) showing different number of ether bridges (EI = 0, 0.2, 0.5, and 1). (C) Schematic model of the conversion (a–d) of a planar oligo BQPo region into a curved stacked BQPoe spiral. Numbers represent EI values. Arrows indicate the direction of the rolling up process.

atoms bound in an infinite hexagonal pattern, at present, attention has turned towards curved graphitic networks such as spherical fullerenes, carbon nanotubes, and onion-like graphitic spheres (Ugarte, 1992). In addition to nano-crystalline graphite regions, TEM studies revealed that carbon black nano- and micro-particles have onion-like structures formed by concentrically arranged graphene sheets (Iijima, 1980). Likewise, stacked planar sheets, soft curved or marked wavy layers, and concentric onion-like
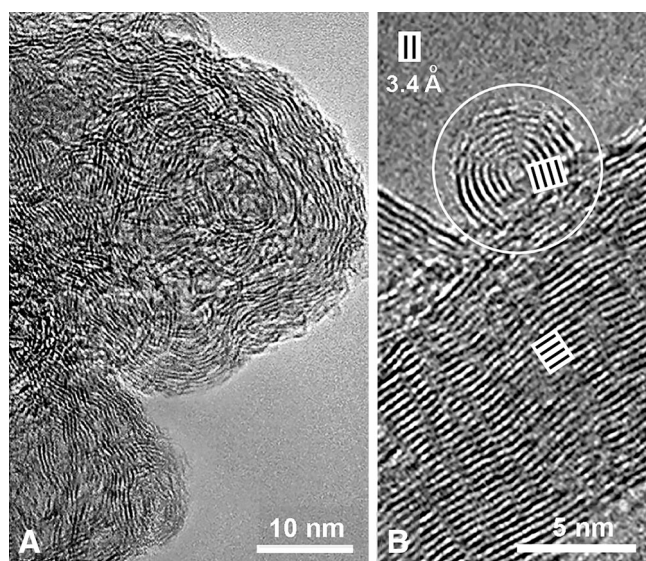

FIGURE 9. (A, B) Transmission electron microscopy (TEM) images of synthetic PDA-melanin, showing (A) a wavy organization of electron dense layers, and (B) strongly curved as well as planar stacked layers, with 3.4 Å interlayer spacing (Reproduced from Chen et al., 2013).

structures are often seen in natural or synthetic eumelanins observed by TEM (Fig. 9), in all cases with a ~3.4 Å-interlayer separation (Cheng et al., 1994; Watt et al., 2009; Chen et al., 2013; Schroeder et al., 2015).

Fullerenes are closed-cage C spheres with great theoretical and practical importance. Regarding nucleation and growth of C60 fullerene (Kroto and McKay, 1988), a curved sheet is first formed due to energy minimization (Ugarte, 1992; Kroto, 1990), and then spiral growth to form a multilayered fullerene continues by wrapping of a hexagonal network with occasional pentagonal rings to optimize curvature (Kroto and McKay, 1988). A partially closed nautilus-like sphere is first formed, and as edge by-pass occurs closure is no longer possible, growth of the curved hemisphere continues to form spiral C nano- and micro-particles (Kroto, 1990).

It is most exciting to consider the possibility that such spiral organization might also occur in the case of eumelanin protomolecules (see Figs. 8(B) and 8(C)). Following the spiral model for nucleation and growth of fullerenes, it is tempting to assume that a similar mechanism may take place to form spiral BQPoe sheets. A supramolecular organization of annular and/or spiral melanin protomolecules could be formed by aggregation of small and then large globular structures, perhaps following co-axial and/or co-lateral (side-to-side) binding. Crystalline C60 (fullerite, Krätschmer et al., 1990), C60 fullerene fibers (Malik et al., 2007), graphite and graphene sponges and cross-linked fullerene frameworks (Nueangnoraj et al., 2013; Bay et al., 2016), onion-like graphitic spheres (Diudea et al., 2014), as well as fulleroids and schwarzites (Avery, 2018) are illustrative examples of possible structures for supramolecular eumelanin organization.

As reviewed by Büngeler et al. (2017), the formation of mammalian and *Sepia* eumelanin involves four steps of hierarchical buildup mechanism. Each step increases the size of the melanin particle in the following way: (a) melanin oligomer sheets produce (b) proto-particles (~2–5 nm) with onion-like structure, which condense into (c) spherical type-A particles (~20–40 nm) that then aggregate in (d) spherical type-B particles (~200 nm). Morphological data indicate that large particles are amorphous aggregates of small globular bodies (Longuet-Higgins, 1960). It is noteworthy the analogous size of a spherical proto-particle (20–50 Å), and the spiral BQPoe model (2 and 4 turns: 21 and 42 Å in diameter, respectively).

This allows to speculate that the supramolecular organization of both natural and synthetic eumelanins derives from fractal aggregates of globular units, the aggregation process involving hydration levels, with low pHs and high ionic strength promoting aggregation to larger structures (Bridelli, 1998). This agrees with the hypothesis advanced by Zeise et al. (1992) of small (proto) particles that are capable of aggregating to build the final eumelanin structure.

According to D'Alba and Shawkey (2019), and Benito-Martínez et al. (2020), melanosomes are formed through four stages identified by TEM. The pre-melanosome Stage I is an endosome budded from the *trans*-Golgi network (TGN), with incipient PMEL17 amyloid-like fibrils; in Stage II, fibrils are assembled into a laminar matrix, formed by regularly spaced sheets; in Stage III, synthesis of electron-dense melanin appears on the β-sheet fibrils of the laminar

matrix; and in Stage IV, deposition of melanin continues until the underlying sheets are completely obscured. Normally, deposition of melanin is limited to Stages III–IV, but tyrosinase activity is early detectable in the TGN; from them, coated vesicles containing the enzyme bud and fusion with stage II melanosomes.

On the basis of chemical and physical data, eumelanin protomolecules would be formed by stacking of four or more sheets (oligomers), with each sheet consisting of 4-16 indole monomers linked together, so that the O atoms lie on the outer edges of the sheet, whereas the N atoms are located in a porphyrin-like hole at the sheet center (Cheng et al., 1994; Zajac et al., 1994; Zecca et al., 2008). The oligomers are then settled in planar graphitic layers or in fullerene-like bodies (Nicolaus, 2005a). Stacked planar or spiral oligo-BQPo units accord with this proposed structural organization of eumelanin. In the local-order-global-disorder model, a combination of π-stacked, hydrogen and ionic bonded nanostructures would be formed, which then aggregate to form disordered spherical particles that aggregate again to form globular structures (Sulzer et al., 2018). Both neuromelanin and eumelanin were claimed to be composed of onion-like concentric circles (Schroeder et al., 2015), which agrees with the idea that the melanin protomolecules could assume a fullerene-like closed form (Olivieri and Nicolaus, 1999; Nicolaus, 2005a), or a spiral globular structure (see Figs. 7 and 8).

Supramolecular Properties

Striking features of eumelanin are broad-band light absorption, efficient dissipation of the absorbed photon energy as heat, semi- and photo-conductivity features, ultrasound absorption, strong binding of metal cations and organic compounds, paramagnetism, reversible redox behavior, antioxidant and radical-scavenger activity, high adhesivity, and ion-exchange reactions. Previous and recent reviews on the chemistry, properties, biotechnological and biomedical applications of melanin and melanin-like materials are available (see Edelstein, 1971; Swan, 1974; Sarangarajan and Apte, 2006; Solano, 2017; Scognamiglio et al., 2017; Huang et al., 2018; D'Alba and Shawkey, 2019; Park et al., 2019; d'Ischia, 2018; Mavridi-Printezi et al., 2020; Galeb et al., 2021; Blázquez-Castro and Stockert, 2021). In what follows, some of these fascinating properties will be elaborated upon.

Spectroscopical features

The brown-black color of eumelanin is a direct evidence of its efficient light absorption (Cavallini et al., 2020). Spectral absorption of mammalian, invertebrate (cuttlefish), and synthetic melanins, as well as carbon black (e.g., China ink) presents similar features, showing a broad-band photonic absorption with exponential decay from the ultraviolet (UV) to visible and near-infrared (NIR) region (Tran et al., 2006; Plaetzer et al., 2009; Micillo et al., 2016; Micillo et al., 2017; Mostert, 2021). This feature reminds more of graphitic materials and inorganic semiconductors with a small Eg (~0.5–1.5 eV) than of organic chromophores with structured absorption peaks, which are typically associated to transitions from π bonding to antibonding π* localized orbitals.

In keeping with this, eumelanins are supramolecular amorphous semiconductors characterized by valence and conduction bands (Nicolaus, 1997; Mavridi-Printezi et al., 2020). These features are also found in graphene and pyrolyzed PDA, as well as carbon spheres and films (Liu et al., 2014). In addition to UV-visible-NIR radiation, eumelanin is capable of absorbing X- and γ-rays (Hill, 1992; Krol and Liebler, 1998), and ultrasound in the MHz range (Kono et al., 1979; Kono et al., 1981; McGinness et al., 1976).

Taking into account the stimulating effect of UV radiation on melanogenesis, UV treatments have been applied to mitigate depigmentation in vitiligo patients. Using several types of phototherapy (psoralen–UVA, narrow-band UVB) has not yet produced a definite cure, although prolonged phototherapy with the latest modality appears encouraging for face and neck vitiligo lesions (Bae et al., 2017).

The amplitude of the Eg in oligomers and unstacked eumelanins is relatively wide, but it diminishes when the conjugation (number of repetitive units) increases, and also when stacking occurs. In this way, the Eg of the pigment reaches the typical narrow values of semiconductor materials (Fig. 10).

Although lower than in monomer precursors, the Eg of oligomers with few indole units is still considerable (Fig. 10(A)). However, with increasing units the separation between the VB and CB becomes smaller and within the semi-conductivity range (Eg ≤ ~4 eV). In the case of oligo-BQPo with ether bridges (BQPoe), Eg depends on the number of bridges. The same behavior of Eg occurs in the case of allomelanin materials (Fig. 10(B)).

Therefore, melanins are similar to conductive and semi-conductive organic polymers such as poly acetylene, poly p-phenylene, poly aniline, poly thiophene, and poly pyrrole (with Eg of 2 eV and 3 eV for the two latter compounds, respectively), co-planarity of aromatic units being a basic requisite (Gardini and Berlin, 1991; Nicolaus, 2005a). Linear semi-conductive polymers, either flexible or rigid, is based on a high π-electron delocalization, and this is just what occurs in the planar poly-BQPo model (see Fig. 3).

Synthetic and natural eumelanins act as an amorphous semiconductor threshold switch. Switching occurs reversibly at potential gradients two to three orders of magnitude lower than reported for inorganic films (McGinness et al., 1974; Filatovs et al., 1976; Nicolaus, 1997; Jastrzebska et al., 2002). In a post-publication note (Mott, 2001), a flash of light (clearly electro-luminescence) was described when melanins switch. The weak electrical conductivity ($\sigma = 10^{-11}$ to 10^{-7} $\Omega^{-1}cm^{-1}$) is increased by formation of charge-transfer complexes, metal doping and included agents, presence of counterions, hydration, light and temperature.

Threshold conductivity switching, photo-conductivity, stable EPR signal, photo-voltaic effect, etc., are conspicuous features but small variations can be found according to the method of synthesis and purification used (Nicolaus, 1997). Black, solid-state amorphous semiconductors have a very narrow Eg (0.1–1.7 eV). An example is the broad-band absorbing fullerene C60 with Eg = 1.7 eV. NIR radiation of 808 nm corresponds to an energy of 1.53 eV.
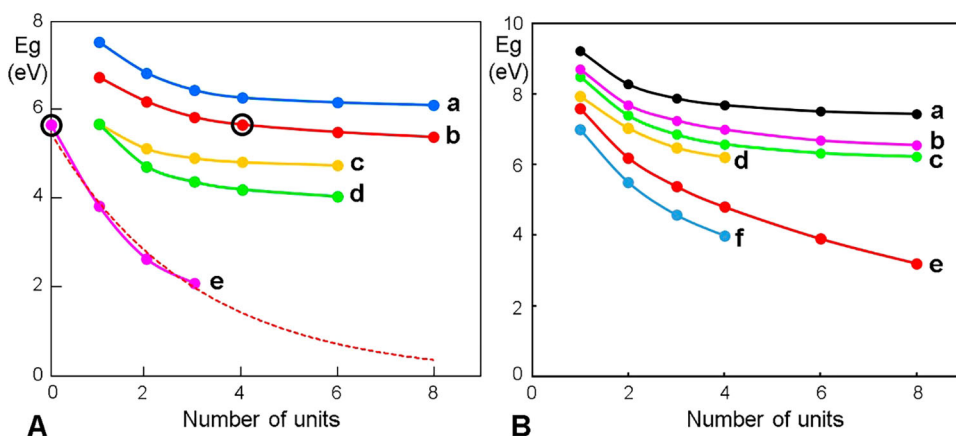
FIGURE 10. Eg curves for melanin models as a function of the number of repetitive units. (A) Eumelanin models with indole units (a–d) or ether bridges (e). (a) 4-7 IQ; (b) BQPo; (c) 3-4 IQ; (d) 1-7,3-4 IQ; and (e) BQPo ethers; in this case, the black circle indicates one BQPo unit without ether bridge. Tetra-BQPo with 3 ether units (EI = 1) has Eg = 2.1 eV. The exponential extrapolation (dashed red curve) shows that with 5 units, Eg would be ~1 eV, and with 50 units, ~0.2 eV. (B) Allomelanin models. (a) 3,4-7,8(1,2,5,6-naphthoquinone); (b) 3-6(1,2,7,8-naphthoquinone); (c) 2-2(o-benzoquinone); (d) 2-5(3,4-dioxopyrrole); (e) 2-7(1,8-naphthoquinone, poly-DHN); and (f) 1-4(2,3-naphthoquinone).

Fluorescence

Eumelanins are capable of dissipating >99.9% of absorbed UV-visible radiation through a non-radiative decay mode (Meredith and Riesz, 2004). Since the radiative decay of excited eumelanin is nearly zero, it is expected that its fluorescence emission should be negligible, as was early pointed out (Thompson, 1966). However, an intriguing autofluorescence has been assigned to melanin (Fellner et al., 1979; Gallas and Eisner, 1987), with an excitation peak at 450 nm and emission from 440 nm to >800 nm. Fluorescence lifetime imaging for ophthalmoscopy, thermophoresis assays of melanin-binding drugs, and detection of melanin in pigmented cells have been reported and assigned to autofluorescence (Fernandes et al., 2016; Dysli et al., 2017; Hellinen et al., 2020).

Although under UV or short visible light, melanin has negligible fluorescence, under 785-nm NIR excitation it shows a very weak broad-band emission between 820 and 920 nm, which is superimposed with the Raman scatter at 880 and 890 nm (Huang et al., 2006). In contrast, a strong yellow autofluorescence of melanins is induced by partial degradation after H_2O_2 oxidation or UV/violet (330–380 nm, 400–440 nm) radiation on natural and synthetic eumelanin, neuromelanin, and pheomelanin (Kayatz et al., 2001; Elleder and Borovanský, 2001). Interestingly, fluorescent quantification of melanin can be made after degradation under oxidative conditions (heating in alkaline H_2O_2) (Rosenthal et al., 1973; Fernandes et al., 2016).

Likewise, the fluorescence of opio-melanins at 440 and 520 nm, is due to low- and middle-molecular weight fractions, respectively, formed during oxidative photo-bleaching (Mosca et al., 1999), whereas the high molecular weight fraction does not fluoresce. A similar process occurs for the eumelanin-like, non-fluorescent, oxidized brown-black DAB polymer. After immunoperoxidase-DAB staining and irradiation with UV light for 2–4 min, positive cells develop a strong yellow fluorescence that is due to the cleavage of the DAB polymer into smaller fluorescent products (Grube, 1980).

On the other hand, a formaldehyde-induced fluorescence (FIF) in human melanocytes was early described and identified as due to the reaction of the aldehyde with DOPA, yielding an isoquinoline derivative (Falck et al., 1965; Rost and Polak, 1969). A green FIF was found in melanin-containing cells from the *tapetum lucidum* layer of the cat eye (Büssow et al., 1980). In this case, the exc/em maxima (430/490 nm) corresponded to those from 5-S-cysteinyl-DOPA component of pheomelanin rather than DOPA. The levels of 5-S-cysteinyl-DOPA in serum and urine were also a sensitive diagnostic method for detection of melanoma metastasis.

Studies using the FIF method (Paul, 1984) indicated that nevus cells are possibly derivatives of normal melanocytes, still showing a dendritic pattern. Photo-historic analysis also showed that the initial growth of melanoma was very protracted, and mistaken for nevi. Although dendritic tumor cells often occur in all types of melanoma, a great number are only visible in lentigo maligna.

In contrast, fluorescence quenching by melanin is now used for reducing the background autofluorescence of *Xenopus laevis* oocytes, thus improving specific signals from fluorescent-labeled probes after injection of mRNA (Lee and Bezanilla, 2019). Two methods were suitable, either using the drug, HG 9-91-01, to stimulate melanin production, or direct injection of synthetic PDA-melanin within oocytes.

Paramagnetism

Mammal-, sepio- and DHI-melanin have a radical-cation nature. About one cationic center for every 6-8 indole units was calculated from chlorine values. Melanins also contain one stable radical (unpaired electron) per 200–300 units, which gives an intense electron paramagnetic (spin) resonance (EPR) signal (Blois et al., 1964; Nicolaus, 2005a). Likewise, synthetic fungal DHN-melanin shows higher paramagnetism and stronger radical scavenging capacity than eumelanin (Longuet-Higgins, 1960).

A method for the unambiguous identification of melanin is just based on the detection of radicals by EPR spectroscopy, and it

can be applied for the recognition of microscopically undetectable melanin in melanomas (Sarna and Swartz, 1978). It is also known that the strong binding of NM to Fe^{3+} and other metals enables both EPR and nuclear magnetic resonance (NMR) detection in the living brain (Sulzer et al., 2018).

In the NM–Fe complex the neuromelanin component contains a stable radical associated with the catechol semiquinone group, and a high spin Fe^{3+}. The two species closely interact, forming a complex used for magnetic resonance imaging (MRI). Sequestering radical-containing NM in an autophagic organelle could be protective against radical damage, whereas the synthesis of NM is thought to be neuroprotective as it removes excess cytosolic dopamine (Sulzer et al., 2018). Among the most versatile platforms, SiO_2 shell nanoparticles coated with Gd^{3+}-chelated synthetic dopa-melanin have been applied for in vivo MRI-fluorescence imaging, as well as to induce antitumoral photothermal effect (Cho et al., 2016).

Metal binding

Metal-chelation by oxygen ligands (e.g., catechol, carbonyl, carboxyl) from melanins allows binding between polymer chains, Mg^{2+} and Ca^{2+} ions being the main cations. Histochemical methodology using selective binding of Ca^{2+} by catechol- or quinone-containing reactive dyes are well known (Stockert and Blázquez-Castro, 2017). It is accepted that the high adhesivity of melanins are based on the presence of catechol and quinone groups (Scognamiglio et al., 2017; Ruiz-Molina et al., 2018; Cavallini et al., 2020; Hauser et al., 2020). In the case of melanin models, side-to-side dimers of different structures (e.g., 1-7, 3-4 IQ or DHI, and BQPo) can be easily formed by edge-to-edge binding of metal cations (Sulzer et al., 2018; Cavallini et al., 2020) (see Fig. 2(H)), in stacked planar, cyclic or spiral configurations.

Native sepiomelanin appears as a Ca and Mg salt. Binding to metal cations include alkali, alkali earth, transition metals, and lanthanides (e.g., Na, K, Mg, Ca, Mn, Fe, Cu, Zn, Cd, Sr, Pb, La, Gd, etc.) (Zecca et al., 2008: d'Ischia et al., 2015; Cho et al., 2016; di Mauro et al., 2017; Sulzer et al., 2018; Cavallini et al., 2020). The amount and binding affinity of melanin can be quite large, binding to Mg^{2+}, Ca^{2+}, Sr^{2+}, and Cu^{2+} being 5, 4, 14 and 34 times stronger than EDTA. For Ca, Mg, Fe, Cu o Zn, the saturation levels of binding are ~3-4 indole units per ion (Mostert, 2021).

Metal-chelation by N ligands in porphyrin-like regions (e.g., cyclic IQ tetramer, porphycene) is possible for the corresponding melanin models. Porphycenes form metal complexes with Al^{3+}, Fe^{2+}, Fe^{3+}, Mn^{2+}, Ni^{2+}, Cu^{2+}, Co^{2+}, Zn^{2+}, Pd^{2+}, etc. (Rubio et al., 2005; Stockert et al., 2007). Doping of eumelanin and synthetic melanin with metal ions allows metal-to-ligand charge transfer complexes (e.g., TiO_2 with the indole unit DHICA), producing nanoplatforms for multimodal imaging and therapeutic applications, enhancing anti-inflammatory and antibacterial activity, and improving photocatalysis, light absorption, and photothermal effect of melanins (Cho et al., 2016; di Mauro et al., 2017; Cavallini et al., 2020).

Staining reactivity

Although eumelanin is a dark pigment, its light microscopic visualization depends on its concentration in the melanosome.

Melanin can also modify the color of bound dyes. Unfortunately, cultured melanomas often show weakly or non-pigmented cells. The well-known B16 melanoma can differ significantly in pigmentation, minimal tumorigenic dose, expression of antigens, growth rate in mice, metastatic potential, etc. (Overwijk and Restifo, 2000). Microscopic analysis of cultured cells should allow the observation of melanosomes (Benito-Martínez et al., 2020), but morphological studies are often not performed or the absence of melanosomes is overlooked.

Although at present, many immunohistochemical methods for diagnosis and prognosis of melanomas are available (Hessler et al., 2020), the classical reaction for detection of melanin by means of silver staining remains useful. In the Fontana–Masson method (Thompson, 1966), the silver diammine cation $(Ag[NH_3]_2)^+$ from an ammoniacal silver nitrate solution is reduced by melanin to colloidal metallic Ag^0 (Bancroft and Gamble, 2008). This argentaffin reaction does not require any developer, and the dark color of the reduced silver directly demonstrates the presence of melanin. In addition, chromaffin cells and lipofuscin pigments are also revealed by this method. On account of their catechol groups, melanin also reduces ferric ferricyanide to Prussian blue at acidic pH (Thompson, 1966), and under acid conditions, the bound Fe^{3+} forms Prussian blue with added potassium ferrocyanide (Perls reaction, Lillie, 1977; Sulzer et al., 2018). Melanoma cells, additionally, can be histochemically detected by tyrosinase assays (Angeletti et al., 2004).

Eumelanin is negatively charged at pH values above 4 (Ball, 2010), and then some staining reactivity is related to its polyanionic nature. After common hematoxylin-eosin staining of tissue sections, melanosomes are visualized by staining with the cationic blue aluminum-hematein, which depends on the binding of Al ions to anionic sites. Other staining reactions are based on the high affinity of eumelanin for metal cations and cationic dyes (basophilia). An example is the iron uptake reaction giving a blue-green color (Thompson, 1966), which is typical of ferric-catechol complexes (Lillie, 1977; Sulzer et al., 2018).

Numerous cationic dyes can stain eumelanin. Examples are methylene blue and toluidine blue that stain the pigment in blue. Nile blue stains melanin dark green but also lipofuscin deposits in a blue color (Lillie, 1977). Pinkus' Giemsa stains melanin in a green-brown color (Thompson, 1966). The precise binding mechanism of cationic dyes to eumelanin has been rather overlooked. Since Lerman's formulation of the intercalative binding mode into DNA (Lerman, 1964), numerous dyes have been found to bind into nucleic acids by intercalation (Stockert, 1985), using strong face-to-face hydrophobic interactions between planar dyes and base pairs.

Therefore, on account of the aromatic and anionic character of eumelanin, intercalation of planar cationic dyes should be the preferential binding mode, as occurs with similar substrates stained by acridine, thiazine, azine, oxazine, and xanthene dyes. The emission of fluorochromes bound or near to eumelanin is quenched (Lee and Bezanilla, 2019), as occurs in the presence of graphene and graphene oxide, which severely quench the emission of attached fluorophores (He et al., 2010).

The copper-phthalocyanine (CuPc) macrocycle is an interesting model dye regarding binding to eumelanin. The

CuPc dye Alcian blue 8GX has been used in TEM studies of PDA-melanin (Chen *et al.*, 2013), but a rather poor increase of electron contrast occurs over the natural contrast of a graphitic structure. Using this dye, a new composite was formed by layer-by-layer film deposition of PDA-melanin and Alcian blue 8GX, which displayed an electrical conductivity 5 orders of magnitude higher than that of pure melanin films (Chen *et al.*, 2013).

In addition to π–π stacking, electrostatic interactions with this and other cationic dyes should also play a role, because of the negative charge of eumelanin at neutral pH. Obviously, positive charges on the phthalocyanine ring itself (e.g., cuprolinic blue and its analogous zinc complex, Scott, 1980; Tas *et al.*, 1983; Juarranz *et al.*, 1987; Tempesti *et al.*, 2008), or on the side chains (e.g., Alcian blue 8GX, Juarranz and Stockert, 1982; Scott, 1996) could be advantageous but not essential for intercalative binding and staining of eumelanin.

On the other hand, the acid dye CuPc tetrasulfonate was found to form stacked aggregates on the external surface of multiwall carbon nanotubes (Hatton *et al.*, 2007). Therefore, three binding modes of CuPc dyes on aromatic polymers could occur, namely (a) intercalation between aromatic planes, (b) aggregation on aromatic surfaces, and (c) mixed binding modes. Distinct spectroscopic features should be observed for each case. Intercalation of inorganic cations (Li^+, K^+) and anions (PF_6^-, BH_4^-) between graphite layers is also possible (Gao *et al.*, 2021; Ko *et al.*, 2021).

Biomedical Applications of Melanin

Examples of biomedical uses of melanins and melanin-like materials are referred in recent reviews (Solano, 2017; Park *et al.*, 2019; Hauser *et al.*, 2020; Galeb *et al.*, 2021). Melanins and melanin-like polymers, either alone or complexed with specific ligands, nanometals and oxides, etc., are now widely applied in biomedicine fields such as imaging procedures, opto-acoustic devises, highly adhesive materials, etc. (Park *et al.*, 2019; Liu *et al.*, 2020; Galeb *et al.*, 2021). At present, the commercial availability of sophisticated fluorescence microscopes has also allowed a flourishing usage of melanins in biotechnology and biomedicine. Therefore, taking advantage of these materials, nanomaterials and nanomedicine have gained considerable interest and is now growing steadily (Sharma and Das, 2019; Park *et al.*, 2021).

Regarding adhesiveness, PDA catechol and amine groups interact with substrate surfaces via chelation, hydrogen bonding, and hydrophobic forces (Solano, 2017; Ruiz-Molina *et al.*, 2018). In keeping with this striking property, a possible use for adhesion of SARS-CoV-2 to allomelanin-impregnated chin straps has been suggested (Stockert and Herkovits, 2021).

Melanin production through recombinant microorganisms is an established biomedical application based on biotechnology. Bacteria can synthesize melanin, for example, *Aeromonas*, *Azospirillum*, *Azotobacter*, *Bacillus*, *Escherichia*, *Klebsiella*, *Legionella*, *Micrococcus*, *Mycobacterium*, *Proteus*, *Pseudomonas*, *Rhizobium*, *Shewanella*, *Streptomyces*, and *Vibrio* (Lin *et al.*, 2005). As human melanin has structural similarity with fungal melanin, the pigment extracted from *Cryptococcus neoformans*

has been used for the production of monoclonal antibodies capable of binding to human melanin, for treating patients with metastatic melanoma (Martínez *et al.*, 2019).

Recently, a mechanism of melanin-mediated host immunity has been proposed for COVID-19, suggesting that melanin can bind and block the active site of serine protease furin, which is needed for viral entry into cells (Paria *et al.*, 2020). However, the used *in silico* analysis could be misleading, because no polymeric model of eumelanin can occupy the suggested small binding site of furin. In this rather polemic article, antiviral, antimicrobial, anti-inflammatory, antitumor, and immuno-stimulating activities of melanins were also proposed (Paria *et al.*, 2020).

Most innovative biomedical applications of eumelanin concern ophthalmoscopy and oncology. In the case of ophthalmoscopic diagnosis (in which the lifetime of autofluorescence from the retinal pigment epithelium is recorded), melanin is commonly reported as the autofluorescent green-yellow fluorophore. However, the most important emission is not due to melanin but to lipofuscin (Dysli *et al.*, 2017), which in the window of 440–470 nm excitation and 410–700 nm emission is the brightest fluorescing agent. Other relevant endogenous fluorophores are NAD(P)H, FAD, collagen, elastin, and carotenoids.

In oncology, promising photochemical and photophysical treatments for melanomas are photodynamic therapy (PDT), photothermal therapy (PTT), and sonodynamic therapy (SDT).

Photodynamic therapy

PDT is an antitumor treatment based on the selective uptake of a photosensitizer within tumor cells followed by a suitable light irradiation, which generates reactive oxygen species (ROS) and/or radicals inducing cell death (Stockert *et al.*, 2004; Plaetzer *et al.*, 2009; Zhang *et al.*, 2018; Baskaran *et al.*, 2018; Wang *et al.*, 2021). PDT and PTT protocols for melanomas can be now used. The strong light absorption of melanin and its anti-oxidant and radical-scavenger capacity could hinder PDT effects on melanoma cells, but advances in PDT applications in melanoma cultures or tumors have been described (Barbazetto *et al.*, 2003; Sheleg *et al.*, 2004; Kolarova *et al.*, 2007; Skidan *et al.*, 2008; Chen *et al.*, 2008; Cook-Moreau *et al.*, 2010; Maduray *et al.*, 2011; Radzi *et al.*, 2012; Baldea and Filip, 2012; Rapozzi *et al.*, 2014; Naidoo *et al.*, 2018; Pereira *et al.*, 2018; Valli *et al.*, 2019; Akasov *et al.*, 2019; Pan *et al.*, 2021).

Recently, Pires *et al.* (2020) applied dual PDT for murine B16-F10 pigmented and B78-H14 non-pigmented melanomas using cellular-PDT with Photodithazine, and vascular-PDT with Visudyne, followed by irradiation with 670 and 690 nm, respectively, with good results. Here, a novel approach was the topical use of optical clearing agents before PDT to improve the light penetration in melanoma tissue.

A recent addition to the stockpile of PDT is upconversion PDT (UC-PDT). This approach takes advantage of the upconversion phenomenon: the emission of more energetic photons (UV-VIS) after two or three less energetic photons (NIR) are absorbed and their energies summed up by certain rare-earth doped materials (Qiu *et al.*, 2018). This UC-PDT has been successfully applied in experimental models of melanoma PDT, both *in vitro* (Lee

et al., 2020) and *in vivo* (Idris *et al.,* 2012). However, it must be noted that upconversion in general and, by extension, UC-PDT rely on light intensities (0.5 Wcm^{-2} and above) that can lead to a direct photothermal action, particularly when a melanotic tumor is the target. Indeed, this is the case for some of the results reported. Idris *et al.* (2012) found that laser illuminating the melanotic tumors without UC nanoparticles induced a notable tumor toxicity. This could only happen due to a photothermal effect, probably driven by melanin absorption of the 980 nm photons employed. In fact, UC nanoparticles have been recently employed to enhance the photothermal effect in a melanoma model due to the efficient NIR-to-heat conversion of these nanoparticles (Krylov *et al.,* 2020). Even more recently, another group has advanced a complementary UC-PDT/UC-PTT approach to maximize the damaging action upon melanoma tumors (Zhong *et al.,* 2021). In our opinion, the intense light fluxes (around Wcm^{-2}) necessary to produce the UC-PDT preclude their successful application in melanotic melanomas because the NIR absorption of melanin will provoke an unavoidable thermal shock in the tissue.

Photothermal therapy
In contrast with the photochemical principle supporting PDT, PTT is an antitumoral therapy based on the physical photothermal effect (light-to-heat conversion) (Parrish *et al.,* 1983; Jori and Spikes, 1990; Camerin *et al.,* 2009). In this case, the generation of ROS is not required for tumor cell death. An efficient photothermal effect requires fast conversion of excited electrons to vibrational excitation states, which then decay with heat production inducing denaturation of macromolecules, vaporization, and acoustic shock-waves.

Eumelanin is practically the ideal photothermal sensitizer, and the massive vibrational decay from photo-excited electrons in melanotic melanomas induces an efficient heating response that results in coagulative necrosis of the tumor (Kostenich *et al.,* 2000; Colombo *et al.,* 2019; Blázquez-Castro and Stockert, 2021). In the case of melanin-PTT, the endogenous chromophore eumelanin is the selective PTT agent for NIR

irradiation (Fig. 11). Control B16-F10 melanoma cells appear with numerous melanosomes showing variable size and shape, whereas after NIR irradiation, massive coagulative necrosis, cell debris, and a large amount of round melanin-containing macrophages (melanophages) are observed, allowing repetitive PTT treatments. Necrotic tumor cells actively attract macrophages through a phosphatidyl-serine-exposure mechanism (Li *et al.,* 2015). This approach has been applied in Au-SiO$_2$ nanoshells-loaded macrophages for NIR-PTT of tumors (Madsen *et al.,* 2015).

Melanin-like materials, colloidal PDA-melanin, and PDA-coated nanoparticles are suitable NIR photothermal agents for *in vivo* cancer therapy, and have increasing interest for applications in nanomedicine (Liu *et al.,* 2013; Yue and Zhao, 2021). The retinal melanin-pigmented epithelium has been proposed as a suitable PTT target for treatment of macular diseases (Roider *et al.,* 2000). An enhanced PTT also occurs after metal binding to melanin (Cavallini *et al.,* 2020).

On account of an adequate ratio between light absorption by PTT agents and light penetration into tissues, the use of 800-nm NIR-laser irradiation is very suitable to induce successful PTT effects (Weissleder, 2001). Glycerol can be applied to reduce light dispersion by the skin over the tumor (Blázquez-Castro *et al.,* 2018). As glycerol is a strong protecting agent against cell hyperthermia (Henle and Warters, 1982), application of a glycerol drop on the depilated skin also avoids the undesired heating and damage of healthy tissues.

In addition to melanins, carbon materials, black pigments and dyes, mixed-valence compounds, and metal nanoparticles show relevant photothermal activity under NIR illumination (Jiang *et al.,* 2013), and could be used to reinforce melanin-PTT. In the case of black pigments, successful PTT responses have been obtained by using graphitic materials such as carbon dots, nanotubes, etc. (Fisher *et al.,* 2010; Zheng *et al.,* 2015; Chen *et al.,* 2016). Simple China ink (carbon black) is a highly effective PTT agent (Blázquez-Castro *et al.,* 2018). Commercial black toners could be suitable, but they have little carbon content, and large quantities of plasticizer additives (styrene acrylate copolymer and polyester resin), and are not adequate for *in vivo* applications. Carbon
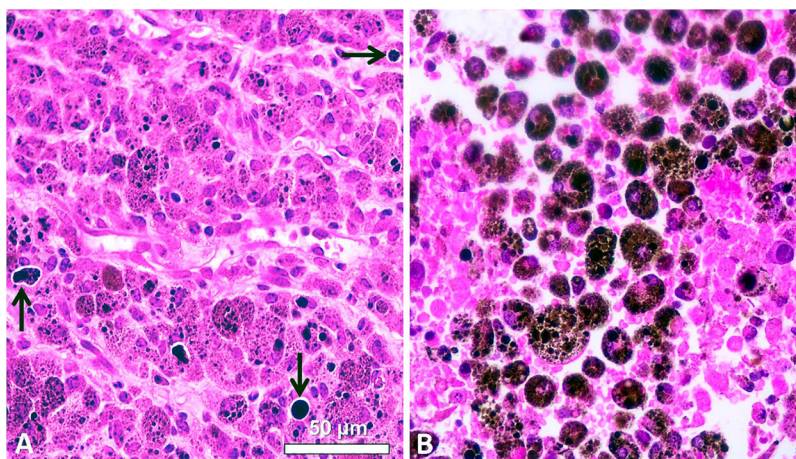

FIGURE 11. H&E images of paraffin sections from B16-F10 murine tumors. (A) Non-irradiated tumor showing polygonal cells, intracellular brown-black melanosomes, and large extracellular melanin granules (arrows). (B) Tumor 24 h after NIR irradiation for 10 min with a portable cw 808-nm laser pointer (200 mW, 1.2 mm beam diameter), showing massive coagulative necrosis: disrupted cells, pycnotic nuclei, and a large amount of round melanin-containing macrophages (melanophages) (Reproduced from Colombo *et al.,* 2019).

quantum dots (<10 nm, obtained from microwave treatment of lemon juice, as well as citric acid, urea, amino acids, etc.) consist of graphitic cores and hydrophilic functionalized shells (Ross et al., 2020), and are very appropriate for PTT of tumors (Sharma and Das, 2019), and sensing toxic metals by fluorescence quenching (Tadesse et al., 2020).

Some Cu(II)-, Ni(II)-, and Pd(II)-containing dyes, such as Cu-hematoporphyrin (Soncin et al., 1999), Ni-octabutoxy-naphthalocyanine (Busetti et al., 1999), and Pd-octabutoxy-naphthalocyanine (Diddens et al., 2003), show NIR-induced photothermal effects. Extensive chemical and mechanical cell damages are caused by the photo-generation of an acoustic shock wave from clusters of aggregated dye within cells (Camerin et al., 2005). Conventional black dyes with canonical absorption spectra, such as Sudan black B, organol black R, amidoblack 10B, aniline blue black, and nigrosine WS (Lillie, 1977; Horobin and Kiernan, 2002) are potential candidates to be used as photothermal agents. The same would be expected for mixed-valence compounds such as ruthenium red, phosphomolybdic blue, Prussian blue, and amylose-iodine inclusion complex (Robin and Day, 1967; Lillie, 1977; Clark, 1984).

Metal and oxide nanoparticles are also currently studied for diagnostic and therapeutic applications (Shi et al., 2015; Li et al., 2018). Administration of gold nanoshells composed of silica cores covered by Au layers to murine colon carcinoma cells followed by 808-nm irradiation resulted in an excellent PTT response (O'Neal et al., 2004). Among other processes, the plasmonic effect induces a photothermal response useful for antitumoral therapy (Carrasco et al., 2020). NIR-laser irradiation of gold (Au) nanoparticles (mainly nanorods, both *in vitro* and *in vivo*, either after intratumoral or intravenous injection) generates a plasmonic photothermal effect (PPTT), which results in cell apoptosis and tumor destruction (Huang and El-Sayed, 2011).

An interesting approach for selective targeted PTT of melanoma cells was described by Lu et al. (2009), using hollow Au nanospheres attached to a ligand peptide (melanocyte-stimulating hormone analog) for receptor-mediated PTT of the B16/F10 melanoma subjected to 808-nm irradiation. The combination of spherical shape, small size (average diameter ~40 nm), absence of silica core, and strong absorption bands in the NIR region makes these nanoparticles ideally suited for PTT.

The analysis of chemical candidates to quickly evaluate a possible PTT effect can be performed using "spot test" on paper strips, followed by NIR laser irradiation. Ignition of blotted papers occurs after few seconds, when temperature reaches 218–246°C, and it is a clear end point of the photothermal reaction. The temperature increase of aqueous solutions of photothermal candidates subjected to irradiation can be also recorded by using a simple mercury thermometer or a thermocouple to assess photothermal responses (Blázquez-Castro et al., 2018; Colombo et al., 2019). Useful biological materials to study mechanisms and applications of melanin-based PTT include bacterial biofilms, 3D melanoma spheroids, and whole organisms such as black amphibian eggs and embryos (*Rhinella*, *Bufo*), black insects (*Aedes aegipty*), plant beans (*Phaseolus vulgaris*), and black seeds (*Sesamum indicum*, *Salvia hispanica*, etc.).

Melanin and ultrasounds

In addition to the biomedical use of ultrasounds (US) in echography, US applications include imaging methods for microscopy, antitumoral high-intensity focused US therapy (HIFU), and sonodynamic therapy. The US microscope uses frequencies near 1,000 MHz, which display viscoelastic properties with a resolution comparable to the light microscope. Sections of normal human retina revealed acoustic attenuation (absorption) in tissue structures such as cell nuclei, rod and cone outer segments, melanin, and red blood cells (Marmor et al., 1977). Comparison of tissue from albino and pigmented rabbits showed that melanin was a particularly strong acoustic attenuator. Photoacoustic signals can also be used to reveal circulating melanoma cells by flow cytometry (O'Brien et al., 2012; Viator et al., 2020).

At present, photoacoustic imaging (PAI) has evolved into a 3D imaging modality (Kratkiewicz et al., 2021). The sample to be imaged is optically excited, leading to a transient temperature rise, with very fast (ps-ns) thermoelastic expansion of the chromophore followed by emission of an acoustic wave. The absorber agent can be endogenous (melanin, hemoglobin, myoglobin, lipid, bilirubin) or exogenous agents such as dyes. Acoustic waves from the absorber are detected by US transducers, generating the absorption map of the tissue. As acoustic waves can traverse longer distances than photons, sensitivity of PAI in deep tissues is orders of magnitude higher than that of pure optical imaging modalities.

In the case of HIFU, a direct and lethal heating of water is obtained focusing high-intensity US into tumor tissue (Lee et al., 2006). However, the melanin content of melanomas strongly absorbs US across several frequencies, and can be used as specific sono-sensitizer (SS). The absorption at 4 MHz has been assigned to molecular motions of a melanin protoparticle with an average molecular weight of ~1.4×10^4 Da (Kono et al., 1981). Interestingly, this value agrees with the molecular weight of a protoparticle modeled as a 4-turn spiral BQPoe (~1.3×10^4 Da). Likewise, the diameter of a protoparticle of PDA-melanin by X-ray diffraction studies is ~30 Å (Chen et al., 1994; Bridelli, 1998), which also corresponds closely to the diameter of a 4-turn spiral BQPoe model (~34.3 Å). In addition, a resonance at 250 MHz was found in melanin associated with stacking of the indole monomer (Kono et al., 1981).

Sonodynamic therapy

An emerging approach for the treatment of atherosclerosis and invasive tumors is sonodynamic therapy (SDT), which involves the use of a SS followed by exposure of the labeled tissue to low intensity ultrasound (US) (Kou et al., 2017; Li et al., 2020; An et al., 2021). Because US has deeper tissue penetration than light, SDT has advantages over PDT and PTT methods. It is accepted that after SDT, tumor cell damage and death are due to generation of ROS and radicals, and then this modality should be better named "sono-electrochemical therapy" (SET), to avoid the misleading use of the term "dynamic". Employed USs are mainly 1–2 MHz and 0.5–10 W/cm^2 (Abrahamse and Hamblin, 2016). Natural SSs such berberine, curcumin, hypericin, and protoporphyrin IX have now increasing importance (Kou et al., 2017; An et al., 2021). Significant regression of experimental melanomas has been

achieved using several SSs such as TiO$_2$ nanoparticles, chloroaluminum phthalocyanine disulfonate, and nickel ferrite/carbon nanocomposites (NiFeO/C), which indicates that SET may be more effective than PDT in treating advanced melanotic melanomas (Li *et al.*, 2020). It is noteworthy that the strong US-absorbing eumelanin from melanomas is just a highly suitable endogenous SS for SET.

Drug and dye binding to melanin
Natural and synthetic melanins are capable of binding other molecules with high dielectric constants (water, dimethyl sulfoxide, formamide, methanol), inducing reversible conductivity changes of as much as ten orders of magnitude (Filatovs *et al.*, 1976). The resistivity of hydrated DOPA-melanin complexed with diethylamine and subjected to US of 10 kHz reduces by ~6 orders of magnitude (Corry *et al.*, 1976). The high affinity of sepia and hair melanins for organic compounds allows to form charge-transfer complexes between the pigment (electron acceptor) and the included compound (electron donor), resulting in a strongly increased conductivity (Nicolaus, 1997).

Both US absorption by melanin, and the number of dead cells do increase sharply with temperature from 7 to 37°C. US absorption is the initial step of the cytotoxic events that convert the phonon energy into cytotoxic products through phonon-electron interactions within the melanosome (Kono *et al.*, 1979). Melanin-binding drugs and dyes induce toxicity in melanocytes subjected to US. Cultured melanotic tumor cells treated with chlorpromazine are preferentially killed by 10 kHz US irradiation (Corry *et al.*, 1976), with radical production appearing involved in DNA damage. Likewise, 1 MHz-US induces melanin degradation and killing of melanin-containing cells, which are strongly potentiated by previous treatment with melanin-binding drugs, such as chlorpromazine and kanamycin (McGinness *et al.*, 1976; Kono *et al.*, 1979).

On the other hand, copper phthalocyanine (CuPc) dyes (e.g., Alcian blue 8GX, Alcian blue pyridine variant, cuprolinic blue, etc.) stain chromatin DNA, and intercalate into nucleic acids duplexes, triplexes and quadruplexes (Juarranz and Stockert, 1982; Stockert, 1985; Juarranz *et al.*, 1987; Scott, 1996; Macii *et al.*, 2020). Therefore, intercalative

binding of these dyes with other aromatic substrates such as eumelanin would be expected to occur, as is the case of Alcian blue 8GX binding to PDA-melanin (Chen *et al.*, 2013). Fig. 12 illustrates this possible binding mode, in which a close molecular fitting occurs between the aromatic CuPc chromophore and two aromatic BQPoe units (Figs. 12(A) and 12(B)), showing fused LUMOs of the intercalation complex (Figs. 12(C)). Intercalative binding of dyes appears as a striking feature of eumelanin, which does not involve structural changes in the X-ray diffraction of the pigment (Thathachari and Blois, 1969), because the dye represents just another aromatic plane.

The high binding affinity of eumelanin for drugs and dyes was found as an unexpected adverse effect of some neuroleptic and antimalarial drugs. Chronic administration of antidepresive phenothiazines (Kinross-Wright, 1956; Burian and Fletcher, 1958) and high-dose chloroquine therapy (Hobbs *et al.*, 1959) produced chorioretinopathy, suggesting an association between toxic effects of some drugs and affinity for eumelanin. Binding of drugs to eumelanin was proved *in silico* by simple free-energy methods, and was also implicated in ototoxicity and disturbances of the skin and hair pigmentation (Raghavan *et al.*, 1990).

Typical dyes and drugs that bind to eumelanin are acridine orange, aflatoxin B$_1$, p-aminobenzoic acid, aminoglycoside and tetracycline antibiotics, bisazo dyes, carcinogenic hydrocarbons, chloroquine, chlorpromazine, dexamethasone, diclofenac, fluorocinolone, fluoroquinolones, herbicides, iodoquine, methotrexate, papaverine, psychotropic and ophthalmic drugs, quinidine, thiazine dyes, thiouracil, thioureas, trimethyl-psoralen, etc. (Potts, 1962; Blois, 1965; Blois and Taskovich, 1969; Lindquist and Ullberg, 1972; Blois, 1972; Lindquist, 1973; Swan, 1974; Larsson, 1991; Larsson, 1993; Lowrey *et al.*, 1997; Jakubiak *et al.*, 2019; Hellinen *et al.*, 2020; Kowalska *et al.*, 2020; Rimpelä *et al.*, 2020). Interestingly, binding of radionuclide-labeled dyes and drugs to eumelanin has been applied for melanoma diagnosis or therapy (Lindquist and Ullberg, 1972; Panasiewicz *et al.*, 1978; Link and Łukiewicz, 1982; Napolitano *et al.*, 1996; Chen *et al.*, 2020).

In the intercalative binding mode, the planar ligand slips between the aromatic units of eumelanin layers from a side
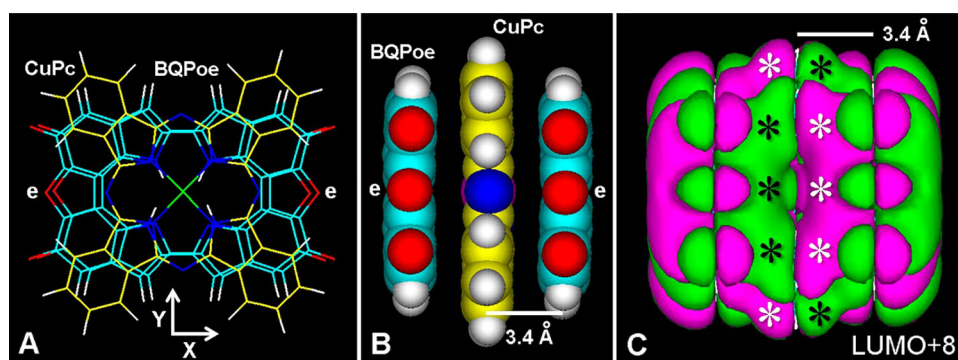

FIGURE 12. (A) Frontal view of the copper-phthalocyanine ring (CuPc, yellow lines) intercalated between two BQPoe units (thin lines) with ether bridges (e), after MM+ energy optimization converged to E = 1 kcal/(Å mol). (B) Lateral (atomic volume, Y axis) view of the intercalated CuPc-BQPoe complex. (C) LUMO+8 (extended Hückel method, Gouraud shaded 3D isosurface, contour: 0.00008, HOMO-0: E = −11.77312 eV, LUMO+0: E = −11.77038 eV, Eg = 0.002 eV). Observe fused MOs (asterisks). The separation between BQPoe and CuPc planes is shown. For element colors see Fig. 3.
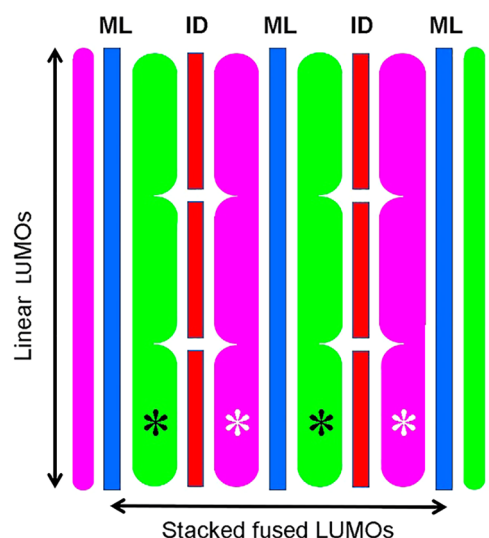
FIGURE 13. Schematic lateral view of intercalated dyes or drugs (ID, red) into melanin layers (ML, blue) of a planar rigid model of eumelanin such as poly-BQPo, showing the linear (vertical), and stacked fused (horizontal) LUMO patterns, with positive (green) and negative (violet) lobes. Asterisks indicate fused LUMOs.

FIGURE 14. Paraffin section of formaldehyde-fixed skin of a southern right whale (*Eubalaena australis*) stained with toluidine blue (50 μg/mL for 10 min), showing the strong and selective metachromatic reaction of melanosomes within keratinocytes (dark violet), and the orthochromatic reaction (blue) of nucleoli (Nu) within nuclei (N). The same pattern is observed after thionine staining. Micro-umbrellas of melanosomes over nuclei are indicated (arrows) (courtesy of M.C. Carou, C.D. Fiorito, and D.M. Lombardo).

edge, and remains trapped as an inclusion complex or "graphitic sandwich", allowing both linear and stacked fused LUMOs (Fig. 13). Numerous dyes and drugs may be used as photo- and sono-sensitizers to enhance the antitumoral activity against melanoma cells, by generating increased and selective photothermal and US electrochemical cytotoxicity, respectively. Suitable dyes for intercalation between aromatic eumelanin layers would be planar vital probes such as acridines, thiazines, porphyrins, phthalocyanines, porphycenes, bisazo dyes, etc.

Acridine orange, toluidine and methylene blue, thionine, Nile blue, TMPyP, ZnTPP, ZnPc, TPPo, PdTPPo, etc., accumulate in endosome-lysosome organelles (Stockert *et al.*, 2004; Stockert *et al.*, 2007), to which also belong melanosomes (Orlow, 1995; Raposo and Marks, 2007). The selective metachromatic staining of skin melanosomes from *Eubalaena australis* with the thiazine dye, toluidine blue, is illustrated in Fig. 14. It is worthy of remark that photo- and sono-active melanin-binding dyes could be the same vital probes commonly used for lysosomes. New developments are expected to occur in these innovative fields of melanosome labeling and physical melanoma therapy.

In all these cases, very small Eg values of dye/drug-melanin complexes allow efficient energy coupling (Corry *et al.*, 1976; McGinness *et al.*, 1976; Crippa *et al.*, 1991), which will result in improved photothermal and US-induced cytotoxicity in melanoma cells. A schematic drawing of possible photon-electron-phonon coupling involving NIR and US radiation followed by thermal and electrochemical responses is shown in Fig. 15.

As US in the MHz range has considerable tissue penetration and is also strongly absorbed by eumelanin, appropriate ligand-eumelanin complexes would give an improved and deeper US therapeutical response, likely due to ROS and radical production (Corry *et al.*, 1976). Therefore, this drug-enhanced SET may represent a more effective and non-invasive treatment for melanoma.
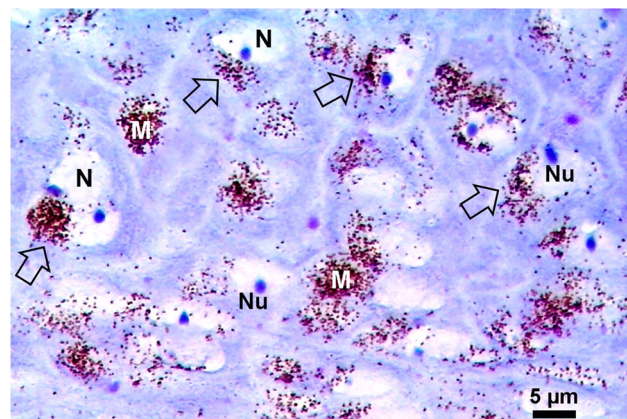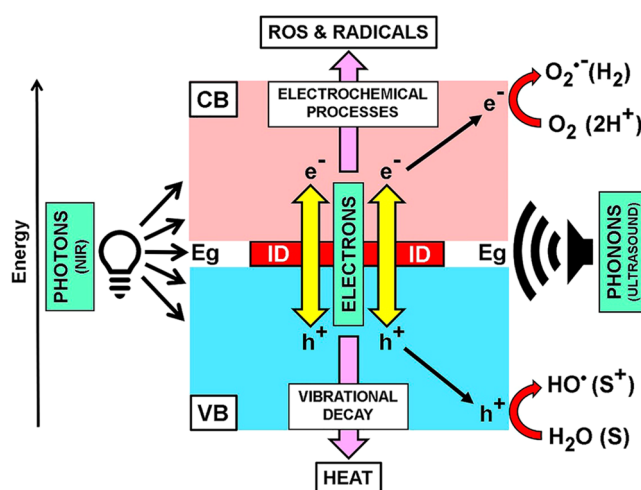

FIGURE 15. Schematic view of the possible "photon-electron-phonon" coupling model for energy interactions in intercalated eumelanin complexes, inspired in concepts from Corry *et al.* (1976), Migliaccio *et al.* (2018), and Sharma and Das (2019). The scheme shows the energy gap (Eg) between VB and CB of eumelanin occupied by a symbolically intercalated dye or drug (ID). Energy decay of photo- or sono-excited π electrons causes vibrational (heat) or electrochemical processes involving electrons (e^-) and holes (h^+), which participate in photo(electro)catalytic redox reactions. Reduction of O_2 to superoxide radical ($O_2^{•-}$) and H_2O_2 proceeds under oxygenated conditions, whereas reduction of protons to H_2 occurs under deoxygenated conditions. Holes can oxidize electron donor substrates (S) to (S^+). All these ROS and radical products generate cell damage and death.

Conclusions and Perspectives

In this review, updated aspects of chemical structures and molecular models of eumelanin have been described, with emphasis on mechanistic parameters related to the main physico-chemical properties and biomedical applications. Rigid and stacked BQPo models, either as planar or curved

sheets, seem to be the best candidates to explain important features of eumelanin, such as broad-band absorption and graphitic structure, semi-conductivity, photothermal and US responses, adhesivity, hydration and dehydration changes, binding to metal ions, drugs and dyes, etc.

Taking into account that it is relatively easy to build feasible molecular models, but difficult to prove such models wrong, and even more difficult to prove them right, the value of the proposed BQPo structures lies in satisfactorily combining a variety of ideas and data to assemble a possible eumelanin organization that make sense in terms of molecular structure and functionality.

The concept of melanosomes as rather inert organelles is in conflict with experimental evidence that show melanins as unusually efficient biopolymer devices for energy conversion. Eumelanins are among the best US-absorbing materials known, and this feature can be applied in US treatments of melanoma. Although there is a lot of progress in melanoma therapy, evolution and prognosis of the advanced disease are still a main concern. Stimulating the scientific discussion will surely lead to novel physical procedures being designed and applied. Melanocytes are killed *in vitro* by 1 MHz-US in proportion to their melanosome content and melanin-included agents. Melanin is a formidable energy absorber of UV-visible-NIR photons and US phonons, and this energy is then converted to tumor cell damaging heat or ROS and radicals.

Organic semi-conductive polymers span from the quantum realm to human disease. Darwin's deaf white kitty illustrates the effect of a strong electron-phonon coupling phenomenon occurring in the inner-ear melanin (Nicolaus, 1997). In addition to strong US-absorbing properties, organic semi-conductive melanins have shown exciting new properties in biotechnology and biomedicine. Examples include organic light-emitting diode displays, melanin-melanoma relationships, deafness, Parkinson disease, and pathological processes based on melanin-drug binding. Melanins are also promising components of electronic circuits, batteries, and solar cells (Ambrico *et al.*, 2011; Migliaccio *et al.*, 2018; Mostert, 2021). Like other light-harvesting biological pigments (e.g., chlorophylls, carotenoids), melanized fungal cells can absorb photon energy from gamma, UV, and visible radiation, and transduce it into life-nurturing metabolic energy (Dadachova *et al.*, 2007; Cordero and Casadevall, 2017). Melanin properties, its applications and possibilities bring upon these ancient and fascinating biopigments a rather renewed interest, as well as very exciting perspectives in biomedical research.

Authors' Contribution: The authors confirm contribution to the paper as follows: study conception and design: J. C. Stockert; draft manuscript preparation, edition and formatting: J. C. Stockert, A. Blázquez-Castro. The authors reviewed the results and approved the final version of the manuscript.

References

Abrahamse H, Hamblin MR (2016). New photosensitizers for photodynamic therapy. *Biochemical Journal* **473**: 347–364. DOI 10.1042/BJ20150942.

Achkar T, Tarhini AA (2017). The use of immunotherapy in the treatment of melanoma. *Journal of Hematology & Oncology* **10**: 5. DOI 10.1186/s13045-017-0458-3.

Ahn A, Chatterjee A, Eccles MR (2017). The slow cycling phenotype: A growing problem for treatment resistance in melanoma. *Molecular Cancer Therapeutics* **16**: 1002–1009. DOI 10.1158/1535-7163.MCT-16-0535.

Akasov RA, Sholina NV, Khochenkov DA, Alova AV, Gorelkin PV, Erofeev AS, Generalova AN, Khaydukov EV (2019). Photodynamic therapy of melanoma by blue-light photoactivation of flavin mononucleotide. *Scientific Reports* **9**: 1–11. DOI 10.1038/s41598-019-46115-w.

Ambrico M, Ambrico PF, Cardone A, Ligonzo T, Cicco SR, Di Mundo R, Augelli V, Farinola GM (2011). Melanin layer on silicon: An attractive structure for a possible exploitation in bio-polymer based metal-insulator–silicon devices. *Advanced Materials* **23**: 3332–3336. DOI 10.1002/adma.201101358.

An YW, Jin HT, Yuan B, Wang JC, Wang C, Liu HQ (2021). Research progress of berberine mediated photodynamic therapy (Review). *Oncology Letters* **21**: 359. DOI 10.3892/ol.2021.12620.

Angeletti C, Khomitch V, Halaban R, Rimm DL (2004). Novel tyramide-based tyrosinase assay for the detection of melanoma cells in cytological preparations. *Diagnostic Cytopathology* **31**: 33–37. DOI 10.1002/(ISSN)1097-0339.

Arad O, Gavaldá A, Rey O, Rubio N, Sánchez-García D et al. (2002). Porficenos para la fotoquimioterapia del cáncer y otras aplicaciones biomédicas. *Afinidad* **59**: 343–356.

Arzillo M, Pezzella A, Crescenzi O, Napolitano A, Land EJ, Barone V, d'Ischia M (2010). Cyclic structural motifs in 5,6-dihydroxyindole polymerization uncovered: Biomimetic modular buildup of a unique five-membered macrocycle. *Organic Letters* **12**: 3250–3253. DOI 10.1021/ol101188c.

Avery JE (2018). Wave equations without coordinates I: Fullerenes. *Rendiconti Lincei. Scienze Fisiche e Naturali* **29**: 609–621. DOI 10.1007/s12210-018-0717-4.

Bae JM, Jung HM, Hong BY, Lee JH, Choi WJ, Lee JH, Kim GM (2017). Phototherapy for vitiligo. *JAMA Dermatology* **153**: 666. DOI 10.1001/jamadermatol.2017.0002.

Baldea I, Filip AG (2012). Photodynamic therapy in melanoma—An update. *Journal of Physiology and Pharmacology* **63**: 109–118.

Ball V (2010). Impedance spectroscopy and zeta potential titration of dopa-melanin films produced by oxidation of dopamine. *Colloids Surface A* **363**: 92–97. DOI 10.1016/j.colsurfa.2010.04.020.

Bancroft JD, Gamble M (2008). *Theory and Practice of Histological Techniques*. (*6th edition*). London: Churchill Livingstone.

Barbazetto IA, Lee TC, Rollins IS, Chang S, Abramson DH (2003). Treatment of choroidal melanoma using photodynamic

therapy. *American Journal of Ophthalmology* **135**: 898–899. DOI 10.1016/S0002-9394(02)02222-5.

Baskaran R, Lee J, Yang SG (2018). Clinical development of photodynamic agents and therapeutic applications. *Biomaterials Research* **22**: 25. DOI 10.1186/s40824-018-0140-z.

Bay HH, Patino D, Mutlu Z, Romero P, Ozkan M, Ozkan CS (2016). Scalable multifunctional ultra-thin graphite sponge: Free-standing, superporous, superhydrophobic, oleophilic architecture with ferromagnetic properties for environmental cleaning. *Scientific Reports* **6**: 21858. DOI 10.1038/srep21858.

Benito-Martínez S, Zhu Y, Jani RA, Harper DC, Marks MS, Delevoye C (2020). Research techniques made simple: Cell biology methods for the analysis of pigmentation. *Journal of Investigative Dermatology* **140**: 257–268. DOI 10.1016/j.jid.2019.12.002.

Berrios-Colon E, Williams S (2012). Melanoma review: Background and treatment. *US Pharmacist* **37**: HS4–HS7.

Bishop CA, Tong LKJ (1964). The reversible addition of hydroxide ion to quinones. *Tetrahedron Letters* **41**: 3043–3046. DOI 10.1016/S0040-4039(01)89438-7.

Blázquez-Castro A, Colombo LL, Vanzulli SI, Stockert JC (2018). NIR pointer laser for *in vivo* photothermal therapy of murine LM3 tumor using intratumoral China ink as a photothermal agent. *Lasers Medical Science* **33**: 1307–1315. DOI 10.1007/s10103-018-2483-z.

Blázquez-Castro A, Stockert JC (2021). Biomedical overview of melanin. 1. Updating melanin biology and chemistry, physico-chemical properties, melanoma tumors, and photothermal therapy. *BIOCELL* **45**: 849–862. DOI 10.32604/biocell.2021.015900.

Blois MS (1965). On chlorpromazine binding *in vivo*. *Journal of Investigative Dermatology* **45**: 475–481.

Blois MS (1972). The binding properties of melanin: *In vivo* and *in vitro*. *Advances in Biology of the Skin* **12**: 65–79.

Blois MS, Taskovich L (1969). The reversible binding of some aromatic and cyclic compounds to biopolymers *in vitro*. *Journal of Investigative Dermatology* **53**: 344–350.

Blois MS, Zahlan AB, Maling JE (1964). Electron spin resonance studies on melanin. *Biophysical Journal* **4**: 471–490. DOI 10.1016/S0006-3495(64)86797-7.

Borovanský J, Wiley I (2011). *Melanins and melanosomes biosynthesis, biogenesis, physiological, and pathological functions*. Germany: John Wiley Distributor. Weinheim, Baden-Württemberg.

Bridelli MG (1998). Self-assembly of melanin studied by laser light scattering. *Biophysical Chemistry* **73**: 227–239. DOI 10.1016/S0301-4622(98)00148-3.

Bridelli MG, Crippa PR, Ugozzoli F (1990). X-ray diffraction studies on melanins in lyophilized melanosomes. *Pigment Cell Research* **3**: 187–191. DOI 10.1111/j.1600-0749.1990.tb00288.x.

Büngeler A, Hämisch B, Strube OI (2017). The supramolecular buildup of eumelanin: Structures, mechanisms, controllability. *International Journal of Molecular Sciences* **18**: 1901.

Burian HM, Fletcher MC (1958). Visual functions in patients with retinal pigmentary degeneration following the use of NP 207. *AMA Archives of Ophthalmology* **60**: 612–629. DOI 10.1001/archopht.1958.00940080632009.

Busetti A, Soncin M, Reddi E, Rodgers MA, Kenney ME, Jori G (1999). Photothermal sensitization of amelanotic melanoma cells by Ni(II)-octabutoxy-naphthalocyanine. *Journal of Photochemistry and Photobiology B: Biology* **53**: 103–109. DOI 10.1016/S1011-1344(99)00132-3.

Büssow H, Baumgarten HG, Hansson C (1980). The tapetal cell: A unique melanocyte in the tapetum lucidum cellulosum of the cat (*Felis domestica* L.). *Anatomy and Embryology* **158**: 289–302. DOI 10.1007/bf00301818.

Camacho E, Vij R, Chrissian C, Prados-Rosales R, Gil D et al. (2019). The structural unit in the cell wall of the fungal pathogen *Cryptococcus neoformans*. *Journal of Biological Chemistry* **295**: 10471–10489. DOI 10.1074/jbc.RA119.008684.

Camerin M, Jori G, Della Ciana J, Fabbroni S, Bonacchi S, Montalti M, Prodi L (2009). Photothermal sensitization and therapeutic properties of a novel far-red absorbing cyanine. *Photochemical and Photobiological Sciences* **8**: 1422–1431. DOI 10.1039/b908495a.

Camerin M, Rello S, Villanueva A, Ping X, Kenney ME, Rodgers MA, Jori G (2005). Photothermal sensitisation as a novel therapeutic approach for tumours: Studies at the cellular and animal level. *European Journal of Cancer* **41**: 1203–1212.

Carrasco E, Stockert JC, Juarranz A, Blázquez-Castro A (2020). Plasmonic hot-electron reactive oxygen species generation: Fundamentals for redox biology. *Frontiers in Chemistry* **8**: 591325. DOI 10.3389/fchem.2020.591325.

Cavallini C, Vitiello G, Adinolfi B, Silvestri B, Armanetti P, Manini P, Pezzella A, d'Ischia M, Luciani G, Menichetti L (2020). Melanin and melanin-like hybrid materials in regenerative medicine. *Nanomaterials* **10**: 1518. DOI 10.3390/nano10081518.

Chen CC, Chen YY, Lo YH, Lin MH, Chang CH, Chen CL, Wang HE, Wu CY (2020). Evaluation of radioiodinated fluoronicotinamide/fluoropicolinamide-benzamide derivatives as theranostic agents for melanoma. *International Journal of Molecular Sciences* **21**: 6597. DOI 10.3390/ijms21186597.

Chen CT, Ball V, de Almeida Gracio JJ, Singh MK, Toniazzo V, Ruch D, Buehler MJ (2013). Self-assembly of tetramers of 5,6-dihydroxyindole explains the primary physical properties of eumelanin: Experiment, simulation, and design. *ACS Nano* **7**: 1524–1532. DOI 10.1021/nn305305d.

Chen CT, Chuang C, Cao J, Ball V, Ruch D, Buehler MJ (2014). Excitonic effects from geometric order and disorder explain broadband optical absorption in eumelanin. *Nature Communications* **5**: 4859. DOI 10.1038/ncomms4859.

Chen L, Malollari KG, Uliana A, Sanchez D, Phillip B, Messersmith PB, Hartwig JF (2021). Selective, catalytic oxidations of C-H bonds in polyethylenes produce functional materials with enhanced adhesion. *Chem* **7**: 137–145. DOI 10.1016/j.chempr.2020.11.020.

Chen Q, Xu L, Liang C, Wang C, Peng R, Liu Z (2016). Photothermal therapy with immune-adjuvant nanoparticles together with checkpoint blockade for effective cancer immunotherapy. *Nature Communications* **7**: 13193. DOI 10.1038/ncomms13193.

Chen Y, Zheng W, Li Y, Zhong J, Ji J, Shen P (2008). Apoptosis induced by methylene-blue mediated photodynamic therapy in melanomas and the involvement of mitochondrial dysfunction revealed by proteomics. *Cancer Science* **99**: 2019–2027. DOI 10.1111/j.1349-7006.2008. 00910.x.

Cheng J, Moss SC, Eisner M (1994). X-ray characterization of melanins-II. *Pigment Cell Research* **7**: 269–273. DOI 10.1111/j.1600-0749.1994.tb00061.x.

Cho S, Park W, Kim DH (2016). Silica-coated metal chelating-melanin nanoparticles as a dual-modal contrast enhancement imaging and therapeutic agent. *ACS Applied Materials & Interfaces* **9**: 101–111. DOI 10.1021/acsami.6b11304.

Clark RJH (1984). The chemistry and spectroscopy of mixed-valence complexes. *Chemical Society Reviews* **13**: 219–244. DOI 10.1039/cs9841300219.

Colombo LL, Vanzulli SI, Blázquez-Castro A, Sanchez Terrero C, Stockert JC (2019). Photothermal effect by 808-nm laser irradiation of melanin: A proof-of-concept study of photothermal therapy using B16-F10 melanotic melanoma growing in BALB/c mice. *Biomedical Optics Express* **10**: 2932–2941. DOI 10.1364/BOE.10.002932.

Cook-Moreau JC, Krausz P, Sturtz FG, Bedane C, Jauberteau-Marchan MO, Ratinaud MH, Bonnetblanc JM (2010). Blue light is phototoxic for B16F10 murine melanoma and bovine endothelial cell lines by direct cytocidal effect. *Anticancer Research* **30**: 143–147.

Cordero RJB, Casadevall A (2017). Functions of fungal melanin beyond virulence. *Fungal Biology Reviews* **31**: 99–112. DOI 10.1016/j.fbr.2016.12.003.

Corry PM, McGinness JE, Armour E (1976). Semiconductor properties of melanins related to preferential killing of melanoma cells. *Pigment Cell* **2**: 321–326.

Cranford S (2021). The ABCs of review articles. *Matter* **4**: 1–3. DOI 10.1016/j.matt.2020.12.013.

Crippa PR, Martini F, Viappiani C (1991). Direct evidence of electron-phonon interaction in melanins. *Journal of Photochemistry and Photobiology B: Biology* **11**: 371–375. DOI 10.1016/1011-1344(91)80042-G.

D'Alba L, Shawkey MD (2019). Melanosomes: Biogenesis, properties, and evolution of an ancient organelle. *Physiological Reviews* **99**: 1–19. DOI 10.1152/physrev.00059.2017.

d'Ischia M (2018). Melanin-based functional materials. *International Journal of Molecular Sciences* **19**: 228. DOI 10.3390/ijms19010228.

d'Ischia M, Wakamatsu K, Cicoira F, di Mauro E, Garcia-Borron JC, Commo S (2015). Melanins and melanogenesis: From pigment cells to human health and technological applications. *Pigment Cell and Melanoma Research* **28**: 520–544. DOI 10.1111/pcmr.12393.

D'Mello SAN, Finlay GJ, Baguley BC, Askarian-Amiri ME (2016). Signaling pathways in melanogenesis. *International Journal of Molecular Sciences* **17**: 1144. DOI 10.3390/ijms17071144.

Dadachova E, Bryan RA, Huang X, Moadel T, Schweitzer AD, Aisen P, Nosanchuk JD, Casadevall A (2007). Ionizing radiation changes the electronic properties of melanin and enhances the growth of melanized fungi. *PLoS One* **2**: e457. DOI 10.1371/journal.pone.0000457.

di Mauro E, Xu R, Soliveri G, Santato C (2017). Natural melanin pigments and their interfaces with metal ions and oxides: Emerging concepts and technologies. *MRS Communications* **7**: 141–151. DOI 10.1557/mrc.2017.33.

Diddens H, Fischer F, Pottier RH (2003). *In-vivo* investigations on dye-enhanced photothermal tumor therapy with a naphthalocyanine derivative. *Oftalmologia* **56**: 59–61.

Diudea MV, Bende A, Nagy CL (2014). Carbon multi-shell cages. *Physical Chemistry Chemical Physics* **16**: 5260–5269. DOI 10.1039/c3cp55309d.

Domingues B, Lopes JM, Soares P, Pópulo H (2018). Melanoma treatment in review. *Immuno Targets and Therapy* **7**: 35–49. DOI 10.2147/ITT.

Dreyer DR, Miller DJ, Freeman BD, Paul DR, Bielawski CW (2012). Elucidating the structure of poly(dopamine). *Langmuir* **28**: 6428–6435. DOI 10.1021/la204831b.

Dreyer DR, Park S, Bielawski CW, Ruoff RS (2010). The chemistry of graphene oxide. *Chemical Society Reviews* **39**: 218–240. DOI 10.1039/B917103G.

Dysli C, Wolf S, Berezin MY, Sauer L, Hammer M, Zinkernagel MS (2017). Fluorescence lifetime imaging ophthalmoscopy. *Progress Retin and Eye Research* **60**: 120–143. DOI 10.1016/j.preteyeres.2017.06.005.

Edelstein LM (1971). Melanin: A unique biopolymer. *Pathobiology Annual* **1**: 309–324.

Eisenman HC, Casadevall A (2012). Synthesis and assembly of fungal melanin. *Applied Microbiological Biotechnology* **93**: 931–940. DOI 10.1007/s00253-011-3777-2.

Elleder M, Borovanský J (2001). Autofluorescence of melanins induced by ultraviolet radiation and near ultraviolet light. A histochemical and biochemical study. *Histochemical Journal* **33**: 273–281. DOI 10.1023/A:1017925023408.

Falck B, Jacobsson S, Olivecrona H, Rorsman H (1965). Pigmented nevi and malignant melanomas as studied with a specific fluorescence method. *Science* **149**: 439–440. DOI 10.1126/science.149.3682.439.

Fellner MJ, Chen AS, Mont M, McCabe J, Baden M (1979). Patterns and intensity of autofluorescence and its relation to melanin in human epidermis and hair. *International Journal of Dermatology* **18**: 722–730. DOI 10.1111/j.1365-4362.1979.tb05009.x.

Fernandes B, Matamá T, Guimaraes D, Gomes A, Cavaco-Paulo A (2016). Fluorescent quantification of melanin. *Pigment Cell & Melanoma Research* **29**: 707–712. DOI 10.1111/pcmr.12535.

Filatovs J, McGinness J, Corry P (1976). Thermal and electronic contributions to switching in melanins. *Biopolymers* **15**: 2309–2312. DOI 10.1002/(ISSN)1097-0282.

Finocchiaro LME, Agnetti L, Fondello C, Glikin GC (2019). Combination of cytokine-enhanced vaccine and chemo-gene therapy as surgery adjuvant treatments for spontaneous canine melanoma. *Gene Therapy* **26**: 418–431. DOI 10.1038/s41434-019-0066-7.

Fisher JW, Sarkar S, Buchanan CF, Szot CS, Whitney J, Hatcher HC, Torti SV, Rylander CG, Rylander MN (2010). Photothermal response of human and murine cancer cells to multiwalled carbon nanotubes after laser irradiation. *Cancer Research* **70**: 9855–9864. DOI 10.1158/0008-5472.CAN-10-0250.

Galeb HA, Wilkinson EL, Stowell AF, Lin H, Murphy ST, Martin-Hirsch PL, Mort RL, Taylor AM, Hardy JG (2021). Melanins as sustainable resources for advanced biotechnological applications. *Global Challenges* **5**: 2000102. DOI 10.1002/gch2.202000102.

Gallas JM, Eisner M (1987). Fluorescence of melanin-dependence upon excitation wavelength and concentration. *Photochemistry and Photobiology* **45**: 595–600. DOI 10.1111/j.1751-1097.1987.tb07385.x.

Galvão DS, Caldas MJ (1990). Theoretical investigation of model polymers for eumelanins. I. Finite and infinite polymers. *Journal of Chemical Physics* **92**: 2630–2636.

Gao T, Han Y, Fraggedakis D, Das S, Zhou T, Yeh CN, Xu S, Chueh WC, Li J, Bazant MZ (2021). Interplay of lithium intercalation and plating on a single graphite particle. *Joule* **5**: 393–414. DOI 10.1016/j.joule.2020.12.020.

Gardini GP, Berlin A (1991). I polimeri conduttori. *La Chimica e l'Industria* **37**: 764–770.

Gingras M (2013). One hundred years of helicene chemistry. Part 3: Applications and properties of carbohelicenes. *Chemical Society Reviews* **42**: 1051–1095. DOI 10.1039/C2CS35134J.

Grube D (1980). Immunoperoxidase methods: Increased efficiency using fluorescence microscopy for 3,3-diaminobenzidine

(DAB) stained semithin sections. *Histochemie* **70**: 19–22. DOI 10.1007/BF00508841.

Hatton RA, Blanchard NP, Stolojian V, Miller AJ, Silva SRP (2007). Nanostructured copper phthalocyanine-sensitized multiwall carbon nanotube films. *Langmuir* **23**: 6424–6430. DOI 10.1021/la070156d.

Hauser D, Septiadi D, Turner J, Petri-Fink A, Rothen-Rutishauser B (2020). From bioinspired glue to medicine: Polydopamine as a biomedical material. *Materials* **13**: 1730. DOI 10.3390/ma13071730.

He S, Song B, Li D, Zhu C, Qi W, Wen Y, Wang L, Song S, Fang H, Fan C (2010). A graphene nanoprobe for rapid, sensitive, and multicolor fluorescent DNA analysis. *Advances in Functional Materials* **20**: 453–459. DOI 10.1002/adfm.200901639.

Hellinen L, Bahrpeyma S, Rimpelä AK, Hagström M, Reinisalo M, Urtti A (2020). Microscale thermophoresis as a screening tool to predict melanin binding of drugs. *Pharmaceutics* **12**: 554. DOI 10.3390/pharmaceutics12060554.

Henle KJ, Warters RL (1982). Heat protection by glycerol *in vitro*. *Cancer Research* **42**: 2171–2176.

Hessler M, Jalilian E, Xu Q, Reddy S, Horton L, Elkin K, Manwar R, Tsoukas M, Mehregan D, Avanaki K (2020). Melanoma biomarkers and their potential application for *in vivo* diagnostic imaging modalities. *International Journal of Molecular Sciences* **21**: 9583. DOI 10.3390/ijms21249583.

Hill HZ (1992). The function of melanin or six blind people examine an elephant. *Bioessays* **14**: 49–56. DOI 10.1002/(ISSN)1521-1878.

Hobbs HE, Sorsby A, Freedman A (1959). Retinopathy following chloroquine therapy. *Lancet* **274**: 478–480. DOI 10.1016/S0140-6736(59)90604-X.

Hong S, Na YS, Choi S, Song IT, Kim WY, Lee H (2012). Non-covalent self-assembly and covalent polymerization co-contribute to polydopamine formation. *Advances in Functional Materials* **22**: 4711–4717. DOI 10.1002/adfm.201201156.

Hong S, Wang Y, Park SY, Lee H (2018). Progressive fuzzy cation-π assembly of biological catecholamines. *Science Advances* **4**: eaat7457. DOI 10.1126/sciadv.aat7457.

Horobin RW, Kiernan JA (2002). *Conn's biological stains. A handbook of dyes, stains and fluorochromes for use in biology and medicine*. 10th edition, Oxford: Bios Scientific Publishers.

Huang L, Liu M, Huang H, Wen Y, Zhang X, Wei Y (2018). Recent advances and progress on melanin-like materials and their biomedical applications. *Biomacromolecules* **19**: 1858–1868. DOI 10.1021/acs.biomac.8b00437.

Huang X, El-Sayed MA (2011). Plasmonic photo-thermal therapy (PPTT). *Alexandria Journal of Medicine* **47**: 1–9. DOI 10.1016/j.ajme.2011.01.001.

Huang Z, Zeng H, Hamzavi I, Alajlan A, Tan E, McLean DI, Lui H (2006). Cutaneous melanin exhibiting fluorescence emission under near-infrared light excitation. *Journal of Biomedical Optics* **11**: 034010–034016. DOI 10.1117/1.2204007.

Idris NM, Gnanasammandhan MK, Zhang J, Ho PC, Mahendran R, Zhang Y (2012). *In vivo* photodynamic therapy using upconversion nanoparticles as remote-controlled nanostructures. *Nature Medicine* **18**: 1580–1585. DOI 10.1038/nm.2933.

Iijima S (1980). Direct observation of the tetrahedral bonding in graphitized carbon black by high resolution electron microscopy. *Journal of Crystal Growth* **50**: 675–683. DOI 10.1016/0022-0248(80)90013-5.

Jakubiak P, Cantrill C, Urtti A, Alvarez-Sánchez R (2019). Establishment of an *in vitro-in vivo* correlation for melanin binding and the extension of the ocular half-life of small-molecule drugs. *Molecular Pharmaceutics* **16**: 4890–4901. DOI 10.1021/acs.molpharmaceut.9b00769.

Jastrzebska M, Kocot A, Tajber L (2002). Photoconductivity of synthetic dopa-melanin polymer. *Journal of Photochemistry and Photobiology B: Biology* **66**: 201–206. DOI 10.1016/S1011-1344(02)00268-3.

Jiang R, Cheng S, Shao L, Ruan Q (2013). Mass-based photothermal comparison among gold nanocrystals, PbS nanocrystals, organic dyes, and carbon black. *Journal of Physical Chemistry C* **117**: 8909–8915.

Jori G, Spikes JD (1990). Photothermal sensitizers: Possible use in tumor therapy. *Journal of Photochemistry and Photobiology, B: Biology* **6**: 93–101. DOI 10.1016/1011-1344(90)85078-B.

Juarranz A, Cañete M, Stockert J (1987). Colour differences in the chromatin staining by cuprolinic blue. *Zeitschrift für mikroskopische-anatomische Forschung* **101**: 532–536.

Juarranz A, Stockert JC (1982). Monastral fast blue. Cytochemical properties of a reaction product from Alcian blue stained chromatin. *Acta Histochemica* **70**: 130–134. DOI 10.1016/S0065-1281(82)80106-2.

Kaxiras E, Tsolakidis A, Zonios G, Meng S (2006). Structural model of eumelanin. *Physical Review Letters* **97**: 218102. DOI 10.1103/PhysRevLett.97.218102.

Kayatz P, Thumann G, Luther TT, Jordan JF, Bartz-Schmidt KU, Esser PJ, Schraermeyer U (2001). Oxidation causes melanin fluorescence. *Investigative Ophthalmology and Visual Sciences* **42**: 241–246.

Kinross-Wright V (1956). Clinical trial of a new phenothiazine compound: NP-207. *Psychiatric Research Reports* **4**: 89–94.

Ko S, Yamada Y, Yamada A (2021). An overlooked issue for high-voltage Li-ion batteries: Suppressing the intercalation of anions into conductive carbon. *Joule* **5**: 998–1009. DOI 10.1016/j.joule.2021.02.016.

Kolarova H, Nevrelova P, Bajgar R, Jirova D, Kejlova K, Strnad M (2007). *In vitro* photodynamic therapy on melanoma cell lines with phthalocyanine. *Toxicology in Vitro* **21**: 249–253. DOI 10.1016/j.tiv.2006.09.020.

Kono R, Yamaoka T, Yoshizaki H, McGinness JE (1979). Anomalous absorption and dispersion of sound waves in diethylamine melanin. *Journal of Applied Physics* **50**: 1236–1244. DOI 10.1063/1.326143.

Kono R, Yoshizaki H, Miyake Y, Izumi Y, McGinness JE (1981). Ultrasonic shear spectrum in hydrated diethylamine melanins and its relation to stacking in a planar group. *Journal of Chemical Physics* **75**: 4654–4660. DOI 10.1063/1.442582.

Kostenich G, Babushkinab T, Malikb Z, Orenstein A (2000). Photothermic treatment of pigmented B16 melanoma using a broadband pulsed light delivery system. *Cancer Letters* **157**: 161–168. DOI 10.1016/S0304-3835(00)00508-5.

Kou JY, Li Y, Zhong ZY, Jiang YQ, Li XS, Han XB, Liu ZN, Tian Y, Yang LM (2017). Berberine-sonodynamic therapy induces autophagy and lipid unloading in macrophage. *Cell Death and Disease* **8**: e2558. DOI 10.1038/cddis.2016.354.

Kowalska J, Banach K, Rok J, Beberok A, Rzepka Z, Wrzesniok D (2020). Molecular and biochemical basis of fluoroquinolones-induced phototoxicity—The study of antioxidant system in human melanocytes exposed to UV-A radiation. *International Journal of Molecular Sciences* **21**: 9714. DOI 10.3390/ijms21249714.

Kratkiewicz K, Manwar R, Zhou Y, Mozaffarzadeh M, Avanaki K (2021). Technical considerations in the Verasonics research ultrasound platform for developing a photoacoustic

imaging system. *Biomedical Optics Express* **12**: 1050–1084. DOI 10.1364/BOE.415481.

Krätschmer W, Lamb LD, Fostiropoulos K, Huffmant DR (1990). Solid C_{60}: A new form of carbon. *Nature* **347**: 354–358. DOI 10.1038/347354a0.

Krieg R, Eitner A, Günther W, Halbhuber KJ (2007). Optimization of heterocyclic 4-hydroxystyryl derivatives for histological localization of endogenous and immunobound peroxidase activity. *Biotechnic & Histochemistry* **82**: 235–262. DOI 10.1080/10520290701714013.

Krol ES, Liebler DC (1998). Photoprotective actions of natural and synthetic melanins. *Chemical Reseacrh and Toxicology* **11**: 1434–1440. DOI 10.1021/tx980114c.

Kroto HW (1990). Fullerene cage clusters. The key to the structure of solid carbon. *Journal of the Chemical Society. Faraday Transactions* **86**: 2465–2468. DOI 10.1039/FT9908602465.

Kroto HW, McKay K (1988). The formation of quasi-icosahedral spiral shell carbon particles. *Nature* **331**: 328–331.

Krylov IV, Akasov RA, Rocheva VV, Sholina NV, Khochenkov DA, Nechaev AV, Melnikova NV, Dmitriev AA, Ivanov AV, Generalova AN, Khaydukov EV (2020). Local overheating of biotissue with upconversion nanoparticles under Yb^{3+} resonance excitation. *Frontiers in Chemistry* **8**: 295. DOI 10.3389/fchem.2020.00295.

Land EJ, Ramsden CA, Riley PA (2004). Quinone chemistry and melanogenesis. *Methods in Enzymology* **378**: 88–109. DOI 10.1016/S0076-6879(04)78005-2.

Larsson BS (1991). Melanin-affinic thioureas as selective melanoma seekers. *Melanoma Research* **1**: 85–90. DOI 10.1097/00008390-199106000-00002.

Larsson BS (1993). Interaction between chemicals and melanin. *Pigment Cell Research* **6**: 127–133. DOI 10.1111/j.1600-0749.1993.tb00591.x.

Lee EEL, Bezanilla F (2019). Methodological improvements for fluorescence recordings in *Xenopus laevis* oocytes. *Journal of General Physiology* **151**: 264–272. DOI 10.1085/jgp.201812189 264.

Lee HM, Hong JH, Choi HI (2006). High-intensity focused ultrasound therapy for clinically localized prostate cancer. *Prostate Cancer and Prostatic Diseases* **9**: 439–443. DOI 10.1038/sj.pcan.4500901.

Lee SY, Lee R, Kim E, Lee S, Park Y (2020). Near-infrared light-triggered photodynamic therapy and apoptosis using upconversion nanoparticles with dual photosensitizers. *Frontiers in Bioengineering and Biotechnology* **8**: 275. DOI 10.3389/fbioe.2020.00275.

Lerman LS (1964). Acridine mutagens and DNA structure. *Journal of Cellular and Comparative Physiology* **64**: 1–18.

Li W, Kim Y, Lee M (2013). Intelligent supramolecular assembly of aromatic block molecules in aqueous solution. *Nanoscale* **5**: 7711. DOI 10.1039/c3nr02574h.

Li XY, Tan LC, Dong LW, Zhang WQ, Shen Lu XX, Zheng X, Lu H, YG (2020). Susceptibility and resistance mechanisms during photodynamic therapy of melanoma. *Frontiers in Oncology* **10**: 1–17. DOI 10.3389/fonc.2020.00597.

Li Z, Venegas V, Nagaoka Y, Morino E, Raghavan P, Audhya A, Nakanishi Y, Zhou Z (2015). Necrotic cells actively attract phagocytes through the collaborative action of two distinct PS-exposure mechanisms. *PLoS Genetics* **11**: e1005285. DOI 10.1371/journal.pgen.1005285.

Li Z, Yu XF, Chu PK (2018). Recent advances in cell-mediated nanomaterial delivery systems for photothermal therapy. *Journal of Materials Chemistry B* **6**: 1296–1311. DOI 10.1039/C7TB03166A.

Liebscher J, Mrówczyński R, Scheidt HA, Filip C, Hädade ND, Turcu R, Bende A, Beck S (2013). Structure of polydopamine: A never-ending story? *Langmuir* **29**: 10539–10548. DOI 10.1021/la4020288.

Lillie RD (1977). *H.J. Conn's Biological Stains. (9th edition).* Baltimore: Williams & Wilkins.

Lin WP, Lai HL, Liu YL, Chiung YM, Shiau CY, Han JM, Yang CM, Liu YT (2005). Effect of melanin produced by a recombinant *Escherichia coli* on antibacterial activity of antibiotics. *Journal of Microbiology, Immunology, and Infection* **38**: 320–326.

Lindgren J, Moyer A, Schweitzer MH, Sjövall P, Uvdal P, Nilsson DE, Kear BP (2015). Interpreting melanin-based coloration through deep time: A critical review. *Proceedings of the Royal Society B: Biological Sciences* **282**: 20150614. DOI 10.1098/rspb.2015.0614.

Lindquist NG (1973). Accumulation of drugs on melanin. *Acta Radiologica: Diagnosis (Stockh)* **325**: 1–92.

Lindquist NG, Ullberg S (1972). The melanin affinity of chloroquine and chlorpromazine studied by whole body autoradiography. *Acta Pharmacologica et Toxicologica* **31**: 1–32. DOI 10.1111/j.1600-0773.1972.tb03310.x.

Link E, Łukiewicz S (1982). A new radioactive drug selectively accumulating in melanoma cells. *European Journal of Nuclear Medicine* **7**: 469–473. DOI 10.1007/bf00253084.

Little WA (1964). Possibility of synthesizing an organic superconductor. *Physical Review* **134**: A1416–A1424.

Liu H, Yang Y, Liu Y, Pan J, Wang J, Man F, Zhang W, Liu G (2020). Melanin-like nanomaterials for advanced biomedical applications: A versatile platform with extraordinary promise. *Advanced Science* **7**: 1903129. DOI 10.1002/advs.201903129.

Liu Y, Ai K, Liu J, Deng M, He Y, Lu L (2013). Dopamine-melanin colloidal nanospheres: An efficient near infrared photothermal therapeutic agent for *in vivo* cancer therapy. *Advanced Materials* **25**: 1353–1359. DOI 10.1002/adma.201204683.

Liu Y, Ai K, Lu L (2014). Polydopamine and its derivative materials: Synthesis and promising applications in energy, environmental, and biomedical fields. *Chemical Reviews* **114**: 5057–5115. DOI 10.1021/cr400407a.

Longuet-Higgins HC (1960). On the origin of the free radical property of melanins. *Archives of Biochemistry and Biophysics* **86**: 231–232. DOI 10.1016/0003-9861(60)90410-0.

Lorquin F, Ziarelli F, Amouric Aès, di Giorgio C, Robin M, Piccerelle P, Lorquin J (2021). Production and properties of non-cytotoxic pyomelanin by laccase and comparison to bacterial and synthetic pigments. *Scientific Reports* **11**: 8538. DOI 10.1038/s41598-021-87328-2.

Lowrey AH, Fameini GR, Loumbev V, Wilson LY, Tosk JM (1997). Modeling drug-melanin interaction with theoretical linear solvation energy relationships. *Pigment Cell Research* **10**: 251–256. DOI 10.1111/j.1600-0749.1997.tb00684.x.

Lu W, Xiong C, Zhang G, Huang Q, Zhang R, Zhang JZ, Li C (2009). Targeted photothermal ablation of murine melanomas with melanocyte-stimulating hormone analog-conjugated hollow gold nanospheres. *Clinical Cancer Research* **15**: 876–886. DOI 10.1158/1078-0432.CCR-08-1480.

Ma K, Li P, Xin JH, Chen Y, Chen Z et al. (2020). Ultrastable mesoporous hydrogen-bonded organic framework-based fiber

composites toward mustard gas detoxification. *Cell Reports Physical Science* 1: 100024. DOI 10.1016/j.xcrp.2020.100024.

Macii F, Arnaiz CP, Arrico L, Busto N, Garcia B, Biver T (2020). Alcian blue pyridine variant interaction with DNA and RNA polynucleotides and G-quadruplexes: Changes in the binding features for different biosubstrates. *Journal of Inorganic Biochemistry* 212: 111199. DOI 10.1016/j.jinorgbio.2020.111199.

Madsen SJ, Christie C, Hong SJ, Trinidad A, Peng Q, Uzal FA, Hirschberg H (2015). Nanoparticle-loaded macrophage-mediated photothermal therapy: Potential for glioma treatment. *Lasers in Medical Sciences* 30: 1357–1365. DOI 10.1007/s10103-015-1742-5.

Maduray K, Karsten A, Odhav B, Nyokong T (2011). *In vitro* toxicity testing of zinc tetrasulfophthalocyanines in fibroblast and keratinocyte cells for the treatment of melanoma cancer by photodynamic therapy. *Journal of Photochemistry and Photobiology B: Biology* 103: 98–104. DOI 10.1016/j.jphotobiol.2011.01.020.

Malik S, Fujita N, Mukhopadhyay P, Goto Y, Kaneko K, Ikeda T, Shinkai S (2007). Creation of 1D [60]fullerene superstructures and its polymerization by γ-ray irradiation. *Journal of Materials Chemistry* 17: 2454–2458. DOI 10.1039/B701583F.

Marmor MF, Wickramasinghe HK, Lemons RA (1977). Acoustic microscopy of the human retina and pigment epithelium. *Investigative Ophthalmology and Visual Sciences* 16: 660–666.

Martínez LM, Martinez A, Gosse G (2019). Production of melanins with recombinant microorganisms. *Frontiers in Bioengineering and Biotechnology* 7: 285. DOI 10.3389/fbioe.2019.00285.

Mavridi-Printezi A, Guernelli M, Menichetti A, Montalti M (2020). Bio-applications of multifunctional melanin nanoparticles: From nanomedicine to nanocosmetics. *Nanomaterials* 10: 2276. DOI 10.3390/nano10112276.

McGinness JE, Corry PM, Armour E (1976). Melanin-binding drugs and ultrasonic-induced cytotoxicity. *Pigment Cell* 2: 316–320.

McGinness JE, Corry PM, Proctor P (1974). Amorphous semiconductor switching in melanins. *Science* 183: 853–855. DOI 10.1126/science.183.4127.853.

Meng S, Kaxiras E (2008). Theoretical models of eumelanin protomolecules and their optical properties. *Biophysical Journal* 94: 2095–2105. DOI 10.1529/biophysj.107.121087.

Meredith P, Riesz J (2004). Radiative relaxation quantum yields for synthetic eumelanin. *Photochemistry and Photobiology* 79: 211–216. DOI 10.1562/0031-8655(2004)079<0211:RCRQYF>2.0.CO;2.

Meredith P, Sarna T (2006). The physical and chemical properties of eumelanin. *Pigment Cell Research* 19: 572–594. DOI 10.1111/j.1600-0749.2006.00345.x.

Micillo R, Panzella L, Iacomino M, Prampolini G, Cacelli I, Ferretti A, Crescenzi O, Koike K, Napolitano A, d'Ischia M (2017). Eumelanin broadband absorption develops from aggregation modulated chromophore interactions under structural and redox control. *Scientific Reports* 7: 41532. DOI 10.1038/srep41532.

Micillo R, Panzella L, Koike K, Monfrecola G, Napolitano A, D'Ischia M (2016). Fifty shades of black and red or how carboxyl groups fine tune eumelanin and pheomelanin properties. *International Journal of Molecular Sciences* 17: 746. DOI 10.3390/ijms17050746.

Migliaccio A, Gryszel M, Đerek V, Pezzella A, Głowacki ED (2018). Aqueous photo(electro)catalysis with eumelanin thin films. *Materials Horizons* 5: 984–990. DOI 10.1039/C8MH00715B.

Mosca L, de Marco C, Fontana M, Rosei MA (1999). Fluorescence properties of melanins from opioid peptides. *Archives of Biochemistry and Biophysics* 371: 63–69. DOI 10.1006/abbi.1999.1403.

Mostert AB (2021). Melanin, the what, the why and the how: An introductory review for materials scientists interested in flexible and versatile polymers. *Polymers* 13: 1670. DOI 10.3390/polym13101670.

Mott N (2001). Nevill Mott's letter on switching in melanins. http://www.drproctor.com/os/mottlet.htm.

Nagasawa Y, Watanabe A, Ando Y, Okada T (2001). Solvent dependence of the ultrafast ground state recovery dynamics of phenol blue. *Journal of Molecular Liquids* 90: 295–302. DOI 10.1016/S0167-7322(01)00133-7.

Naidoo C, Kruger CA, Abrahamse H (2018). Photodynamic therapy for metastatic melanoma treatment: A review. *Technology in Cancer Research & Treatment* 17: 1–15. DOI 10.1177/1533033818791795.

Napolitano A, Palumbo A, d'Ischia M, Prota G (1996). Mechanism of selective incorporation of the melanoma seeker 2-thiouracil into growing melanin. *Journal of Medicinal Chemistry* 39: 5192–5201. DOI 10.1021/jm9605243.

Nicolaus RA (1997). Coloured organic semiconductors: Melanins. *Rendiconto dell' Accademia delle Scienze Fisiche e Matematiche, Napoli* 64: 325–360.

Nicolaus RA (2005a). Perspectives in melanin chemistry. http://www.tightrope.it/nicolaus/link%2023.htm.

Nicolaus BJR (2005b). A critical review of the function of neuromelanin and an attempt to provide a unified theory. *Medical Hypotheses* 65: 791–796. DOI 10.1016/j.mehy.2005.04.011.

Nicolaus RA, Piatelli M, Fattorusso E (1994). The structure of melanins and melanogenesis. IV. On some natural melanins. *Tetrahedron* 20: 1163–1172.

Nueangnoraj K, Nishihara H, Imai K, Itoi H, Ishii T, Kiguchi M, Sato Y, Terauchi M, Kyotani T (2013). Formation of crosslinked-fullerene-like framework as negative replica of zeolite Y. *Carbon* 62: 455–464. DOI 10.1016/j.carbon.2013.06.033.

O'Neal DP, Hirsch LR, Halas NJ, Payne JD, West JL (2004). Photo-thermal tumor ablation in mice using near infrared-absorbing nanoparticles. *Cancer Letters* 209: 171–176.

O'Brien CM, Rood KD, Bhattacharyya K, DeSouza T, Sengupta S, Gupta SK, Mosley JD, Goldschmidt BS, Sharma N, Viator JA (2012). Capture of circulating tumor cells using photoacoustic flowmetry and two phase flow. *Journal of Biomedical Optics* 17: 061221.

Olivieri M, Nicolaus RA (1999). Sulla DHI-melanina. *Rendiconto dell'Accademia delle Scienze Fisiche e Matematiche. Napoli* 66: 85–96.

Orlow SJ (1995). Melanosomes are specialized members of the lysosomal lineage of organelles. *Journal of Investigative Dermatology* 105: 3–7. DOI 10.1111/1523-1747.ep12312291.

Overwijk WW, Restifo NP (2000). B16 as a mouse model for human melanoma. *Current Protocols in Immunology* 39: 20–21. DOI 10.1002/0471142735.im2001s39.

Pan Z, Fan J, Xie Q, Zhang X, Zhang W, Ren Q, Li M, Zheng Q, Lu J, Li D (2021). Novel sulfonamide porphyrin TBPoS-2OH used in photodynamic therapy for malignant melanoma. *Biomedicine and Pharmacotherapy* 133: 111042.

Panasiewicz J, Rybakow Z, Kaskiewicz M, Wiza J (1978). Preparation of ^{35}S labelled methylene blue. *Radiochemical and Radioanalytical Letters* 33: 397–402.

Panzella L, Ebato A, Napolitano A, Koike K (2018). The late stages of melanogenesis: Exploring the chemical facets and the application opportunities. *International Journal of Molecular Sciences* **19**: 1753. DOI 10.3390/ijms19061753.

Paria K, Paul D, Chowdhury T, Pyne S, Chakraborty R, Mandal SM (2020). Synergy of melanin and vitamin-D may play a fundamental role in preventing SARS-CoV-2 infections and halt COVID-19 by inactivating furin protease. *Translational Medicine Communications* **5**: 21. DOI 10.1186/s41231-020-00073-y.

Park J, Lee YK, Park IK, Hwang SR (2021). Current limitations and recent progress in nanomedicine for clinically available photodynamic therapy. *Biomedicines* **9**: 85. DOI 10.3390/biomedicines9010085.

Park J, Moon H, Hong S (2019). Recent advances in melanin-like nanomaterials in biomedical applications: A mini review. *Biomaterials Research* **23**: 24. DOI 10.1186/s40824-019-0175-9.

Parrish JA, Anderson RR, Harrist T, Paul B, Murphy GF (1983). Selective thermal effects with pulsed irradiation from lasers: From organ to organelle. *Journal of Investigative Dermatology* **80**: 75s–80s. DOI 10.1038/jid.1983.19.

Paul E (1984). Malignant melanoma and nevocellular nevi. Histogenesis and relationships. Fluorescence-microscopic and catamnestic photographic studies. *Normal and Pathological Anatomy* **48**: 1–112.

Pereira NM, Laranjo M, Pina J, Oliveira ASR, Ferreira JD et al. (2018). Advances on photodynamic therapy of melanoma through novel ring-fused 5,15-diphenylchlorins. *European Journal of Medicinal Chemistry* **146**: 395–408. DOI 10.1016/j.ejmech.2017.12.093.

Pires L, Demidov V, Wilson BC, Salvio AG, Moriyama L, Bagnato VS, Vitkin IA, Kurachi C (2020). Dual-agent photodynamic therapy with optical clearing eradicates pigmented melanoma in preclinical tumor models. *Cancers* **12**: 1956. DOI 10.3390/cancers12071956.

Plaetzer K, Krammer B, Berlanda J, Berr F, Kiesslich T (2009). Photophysics and photochemistry of photodynamic therapy: Fundamental aspects. *Lasers in Medical Sciences* **24**: 259–268. DOI 10.1007/s10103-008-0539-1.

Potts AM (1962). Uveal pigment and phenothiazine compounds. *Transactions of the American Ophthalmology Society* **60**: 517–552.

Prota G (1997). Pigment cell research: What directions? *Pigment Cell Research* **10**: 5–11. DOI 10.1111/j.1600-0749.1997.tb00460.x.

Prota G (2000). Melanins, melanogenesis and melanocytes: Looking at their functional significance from the chemist's viewpoint. *Pigment Cell Research* **13**: 283–293. DOI 10.1034/j.1600-0749.2000.130412.x.

Qiu H, Tan M, Ohulchanskyy TY, Lovell JF, Chen G (2018). Recent progress in upconversion photodynamic therapy. *Nanomaterials* **8**: 344. DOI 10.3390/nano8050344.

Radzi R, Osaki T, Tsuka T, Magawa TI, Minami S, Okamoto Y (2012). Morphological study in B16F10 murine melanoma cells after photodynamic hyperthermal therapy with indocyanine green (ICG). *Journal of Veterinary Medical Science* **74**: 465–472. DOI 10.1292/jvms.11-0467.

Raghavan PR, Zane PA, Tripp SL (1990). Calculation of drug-melanin binding energy using molecular modeling. *Experientia* **46**: 77–80. DOI 10.1007/BF01955422.

Raposo G, Marks MS (2007). Melanosomes—Dark organelles enlighten endosomal membrane transport. *Nature Reviews Molecular and Cell Biology* **8**: 786–797. DOI 10.1038/nrm2258.

Rapozzi V, Zorzet S, Zacchigna M, Della Pietra E, Cogoi S, Xodo LE (2014). Anticancer activity of cationic porphyrins in melanoma tumour-bearing mice and mechanistic *in vitro* studies. *Molecular Cancer* **13**: 75. DOI 10.1186/1476-4598-13-75.

Rimpelä AK, Garneau M, Baum-Kroker KS, Schönberger T, Runge F, Sauer A (2020). Quantification of drugs in distinctly separated ocular substructures of albino and pigmented rats. *Pharmaceutics* **12**: 1174. DOI 10.3390/pharmaceutics12121174.

Robin MB, Day P (1967). Mixed valence chemistry: A survey and classification. *Advances in Inorganic Chemistry and Radiochemistry* **10**: 247–422. DOI 10.1016/S0065-2792(08)60179-X.

Roider J, Brinkmann R, Wirbelauer C, Laqua H, Birngruber R (2000). Subthreshold retinal pigment epithelium photocoagulation in macular diseases: A pilot study. *British Journal of Ophthalmology* **84**: 40–47. DOI 10.1136/bjo.84.1.40.

Rosenthal MH, Kreider JW, Shiman R (1973). Quantitative assay of melanin in melanoma cells in culture and in tumors. *Analytical Biochemistry* **56**: 91–99. DOI 10.1016/0003-2697(73)90173-5.

Ross S, Wu RS, Wei SC, Ross GM, Chang HT (2020). The analytical and biomedical applications of carbon dots and their future theranostic potential: A review. *Journal of Food and Drug Analysis* **28**: 678–696. DOI 10.38212/2224-6614.1154.

Rost FWD, Polak JM (1969). Fluorescence microscopy and microspectrofluorimetry of malignant melanomas, naevi and normal melanocytes. *Virchows Archiv Abteilung A Pathologische Anatomie* **347**: 321–326. DOI 10.1007/bf00542675.

Rubio N, Prat F, Bou N, Borrell JI, Teixidó J, Villanueva A, Juarranz A, Cañete M, Stockert JC, Nonell N (2005). A comparison between the photophysical and photosensitising properties of tetraphenyl porphycenes and porphyrins. *New Journal of Chemistry* **29**: 378–384. DOI 10.1039/B415314F.

Rughani MG, Gupta A, Middleton MA (2013). New treatment approaches in melanoma: Current research and clinical prospects. *Therapeutic Advances in Medical Oncology* **5**: 73–80. DOI 10.1177/1758834012463260.

Ruiz-Molina D, Saiz Poseu J, Busque F, Nador F, Mancebo J (2018). The chemistry behind catechol-based adhesion. *Angewandte Chemie International Edition* **58**: 696–714. DOI 10.1002/anie.201801063.

Ryu JH, Hong DJ, Lee M (2008). Aqueous self-assembly of aromatic rod building blocks. *Chemical Communications* **2018**: 1043–1054. DOI 10.1039/b713737k.

Sarangarajan R, Apte SP (2006). The polymerization of melanin: A poorly understood phenomenon with egregious biological implications. *Melanoma Research* **16**: 3–10. DOI 10.1097/01.cmr.0000195699.35143.df.

Sarna S, Swartz HM (1978). Identification and characterization of melanin in tissues and body fluids. *Folia Histochemica et Cytochemica* **16**: 275–286.

Schroeder RL, Double KL, Gerber JP (2015). Using sepia melanin as a PD model to describe the binding characteristics of neuromelanin—A critical review. *Journal of Chemical Neuroanatomy* **64–65**: 20–32. DOI 10.1016/j.jchemneu.2015.02.001.

Scognamiglio F, Travan A, Turco G, Borgogna M, Marsich E, Pasqua M, Paoletti S, Donati I (2017). Adhesive coatings based on melanin-like nanoparticles for surgical membranes. *Colloids and Surfaces B: Biointerfaces* **155**: 553–559. DOI 10.1016/j.colsurfb.2017.04.057.

Scott JE (1980). The molecular biology of histochemical staining by cationic phthalocyanine dyes: The design of replacements for Alcian blue. *Journal of Microscopy* **119**: 373–381. DOI 10.1111/j.1365-2818.1980.tb04108.x.

Scott JE (1996). Alcian blue. Now you see it, now you don't. *European Journal of Oral Sciences* **104**: 2–9. DOI 10.1111/j.1600-0722.1996.tb00038.x.

Sharma A, Das J (2019). Small molecules derived carbon dots: Synthesis and applications in sensing, catalysis, imaging, and biomedicine. *Journal of Nanobiotechnology* **17**: 92. DOI 10.1186/s12951-019-0525-8.

Sheleg SV, Zhavrid EA, Khodina TV, Kochubeev GA, Istomin YP, Chalov VN, Zhuravkin IN (2004). Photodynamic therapy with chlorin e6 for skin metastases of melanoma. *Photodermatology, Photoimmunology and Photomedicine* **20**: 21–26. DOI 10.1111/j.1600-0781.2004.00078.x.

Shi D, Sadat ME, Dunn AW, Mast DB (2015). Photo-fluorescent and magnetic properties of iron oxide nanoparticles for biomedical applications. *Nanoscale* **7**: 8209–8232. DOI 10.1039/C5NR01538C.

Simon JD, Hong L, Peles DN (2008). Insights into melanosomes and melanin from some interesting spatial and temporal properties. *Journal of Physical Chemistry B* **112**: 13201–13217. DOI 10.1021/jp804248h.

Skidan I, Dholakia P, Torchilin VP (2008). Photodynamic therapy of experimental B-16 melanoma in mice with tumor-targeted 5,10,15,20-tetraphenylporphin-loaded PEG-PE micelles. *Journal of Drug Targeting* **16**: 486–493. DOI 10.1080/10611860802102175.

Solano F (2017). Melanin and melanin-related polymers as materials with biomedical and biotechnological applications—Cuttlefish ink and mussel foot proteins as inspired biomolecules. *International Journal of Molecular Sciences* **18**: 1561. DOI 10.3390/ijms18071561.

Soncin M, Busetti A, Fusi F, Jori G, Rodgers MA (1999). Irradiation of amelanotic melanoma cells with 532 nm high peak power pulsed laser radiation in the presence of the photothermal sensitizer Cu(II)-hematoporphyrin: A new approach to cell photoinactivation. *Phochemistry and Photobiology* **69**: 708–712. DOI 10.1111/j.1751-1097.1999.tb03351.x.

Stockert JC (1985). Cytochemistry of nucleic acids: Binding mechanisms of dyes and fluorochromes. *BIOCELL* **9**: 89–131.

Stockert JC (2021). Melanin and melanoma: Updating molecular structure and photothermal therapy. *InVet* **23**: 1–15. http://www.fvet.uba.ar/archivos/publicaciones/invet/vol23-1-2021/art-4-vol23-1-2021.pdf.

Stockert JC, Abasolo MI (2011). Inaccurate chemical structure of dyes and fluorochromes found in the literature can be problematic for teaching and research. *Biotechnic and Histochemistry* **86**: 52–60. DOI 10.3109/10520295.2010.489428.

Stockert JC, Blázquez-Castro A (2017). *Fluorescence Microscopy in Life Sciences, E-Book*. Sharjah: Bentham Science Publishers.

Stockert JC, Cañete M, Juarranz A, Villanueva A, Horobin RH, Borrell JI, Teixidó J, Nonell S (2007). Porphycenes: Facts and prospects in photodynamic therapy of cancer. *Current Medicinal Chemistry* **14**: 997–1026. DOI 10.2174/092986707780362934.

Stockert JC, Herkovits J (2021). Melanin adhesivity for possible trapping of SARS-CoV-2 on chin straps: A proof-of-concept assay using model nanoparticles. *Acta Scientific Microbiology* **4**: 2–5. DOI 10.31080/ASMI.2020.04.0759.

Stockert JC, Juarranz A, Villanueva A, Nonell S, Horobin RW et al. (2004). Photodynamic therapy: Selective uptake of photosensitizing drugs into tumor cells. *Current Topics in Pharmacology* **8**: 185–217.

Sulzer D, Cassidy C, Horga G, Kang UJ, Fahn S et al. (2018). Neuromelanin detection by magnetic resonance imaging (MRI) and its promise as a biomarker for Parkinson's disease. *NPJ Parkinson's Disease* **4**: 1–13. DOI 10.1038/s41531-018-0047-3.

Swan GA (1974). Structure, chemistry, and biosynthesis of the melanins. *Fortschritte der Chemie Organischer Naturstuffe* **31**: 522–582. DOI 10.1007/978-3-7091-7094-6.

Swift JA (2009). Speculations on the molecular structure of eumelanin. *International Journal of Cosmetic Science* **31**: 143–150. DOI 10.1111/j.1468-2494.2008.00488.x.

Tadesse A, Hagos M, RamaDevi D, Basavaiah K, Belachew N (2020). Fluorescent-nitrogen-doped carbon quantum dots derived from citrus lemon juice: Green synthesis, mercury(II) ion sensing, and live cell imaging. *ACS Omega* **5**: 3889–3898. DOI 10.1021/acsomega.9b03175.

Tas J, Mendelson D, van Noorden CJF (1983). Cuprolinic blue: A specific dye for single-stranded RNA in the presence of magnesium chloride. I. Fundamental aspects. *Histochemical Journal* **15**: 801–814.

Tempesti TC, Stockert JC, Durantini EN (2008). Photosensitization ability of a water soluble zinc(II) tetramethyltetrapyridino porphyrazinium salt in aqueous solution and biomimetic reverse micelles medium. *Journal of Physical Chemistry B* **112**: 15701–15707. DOI 10.1021/jp808094q.

Thathachari YT, Blois MS (1969). Physical studies on melanins. II. X-ray diffraction. *Biophysical Journal* **9**: 77–89.

Thompson SW (1966). *Selected Histochemical and Histopathological Methods*. Springfield, Illinois: C.C. Thomas.

Tran ML, Powell BJ, Meredith P (2006). Chemical and structural disorder in eumelanins: A possible explanation for broadband absorbance. *Biophysical Journal* **90**: 743–752. DOI 10.1529/biophysj.105.069096.

Ugarte D (1992). Curling and closure of graphitic networks under electron-beam irradiation. *Nature* **359**: 707–709. DOI 10.1038/359707a0.

Valli F, García Vior MC, Roguin LP, Marino J (2019). Oxidative stress generated by irradiation of a zinc(II) phthalocyanine induces a dual apoptotic and necrotic response in melanoma cells. *Apoptosis* **24**: 119–134. DOI 10.1007/s10495-018-01512-w.

Viator JA, Hazur M, Sajewski A, Tarhini A, Sanders ME, Edgar RH (2020). Photoacoustic detection of circulating melanoma cells in late stage patients. *Journal of Innovative Optical Health Sciences* **13**: 2050023. DOI 10.1142/S1793545820500236.

Wang Y, You W, Li X (2020). Current status of gene therapy in melanoma treatment. *BIOCELL* **44**: 167–174. DOI 10.32604/biocell.2020.09023.

Wang Z, Peng H, Shi W, Gan L, Zhong L et al. (2021). Application of photodynamic therapy in cancer: Challenges and advancements. *BIOCELL* **45**: 489–500. DOI 10.32604/biocell.2021.014439.

Wasmeier C, Hume AN, Bolasco G, Seabra MC (2008). Melanosomes at a glance. *Journal of Cell Science* **121**: 3995–3999. DOI 10.1242/jcs.040667.

Watt AAR, Bothma JP, Meredith P (2009). The supramolecular structure of melanin. *Soft Matter* **5**: 3754–3760. DOI 10.1039/b902507c.

Weissleder R (2001). A clearer vision for *in vivo* imaging. *Nature Biotechnology* **19**: 316–317. DOI 10.1038/86684.

Wiriyasermkul P, Moriyama S, Nagamori S (2020). Membrane transport proteins in melanosomes: Regulation of ions for pigmentation. *Biochimica Biophysica Acta Biomembranes* **1862**: 183318. DOI 10.1016/j.bbamem.2020.183318.

Yue Y, Zhao X (2021). Melanin-like nanomedicine in photothermal therapy applications. *International Journal of Molecular Sciences* **22**: 399. DOI 10.3390/ijms22010399.

Zajac GW, Gallas JM, Cheng J, Eisner M, Moss SC, Alvarado-Swaisgood AE (1994). The fundamental unit of synthetic melanin: A verification by tunneling microscopy of X-ray scattering results. *Biochimica et Biophysica Acta—General Subjects* **1199**: 271–278. DOI 10.1016/0304-4165(94)90006-X.

Zecca L, Bellei C, Costi P, Albertini A, Monzani E et al. (2008). New melanic pigments in the human brain that accumulate in aging and block environmental toxic metals. *Proceedings of the National Academy of Sciences USA* **105**: 17567–17572. DOI 10.1073/pnas.0808768105.

Zeise L, Addison RB, Chedekel MR (1992). Bio-analytical studies of eumelanins. I. Characterization of melanin the particle.

Pigment Cell Research **3**: 48–53. DOI 10.1111/j.1600-0749.1990.tb00348.x.

Zhang J, Jianga C, Figueiró Longo JP, Azevedo RB, Zhang H, Muehlmann LA (2018). An updated overview on the development of new photosensitizers for anticancer photodynamic therapy. *Acta Pharmaceutica Sinica B* **8**: 137–146. DOI 10.1016/j.apsb.2017.09.003.

Zheng R, Wang S, Tian Y, Jiang X, Fu D, Shen S, Yang W (2015). Polydopamine-coated magnetic composite particles with an enhanced photothermal effect. *ACS Applied Materials and Interfaces* **7**: 15876–15884. DOI 10.1021/acsami.5b03201.

Zhong Y, Zhang X, Yang L, Liang F, Zhang J, Jiang Y, Chen X, Ren F (2021). Hierarchical dual-responsive cleavable nanosystem for synergetic photodynamic/photothermal therapy against melanoma. *Materials Science & Engineering C* **131**: 112524. DOI 10.1016/j.msec.2021.112524.

Zhou X, McCallum NC, Hu Z, Cao W, Gnanasekaran K, Feng Y, Stoddart JF, Wang Z, Gianneschi NC (2019). Artificial allomelanin nanoparticles. *ACS Nano* **13**: 10980–10990. DOI 10.1021/acsnano.9b02160.